

A Nonlocal Denoising Algorithm for Manifold-Valued Images Using Second Order Statistics

Extended Version

Friederike Laus*, Mila Nikolova[†], Johannes Persch*, and Gabriele Steidl*

December 14, 2016

Abstract

Nonlocal patch-based methods, in particular the Bayes' approach of Lebrun, Buades and Morel [41], are considered as state-of-the-art methods for denoising (color) images corrupted by white Gaussian noise of moderate variance. This paper is the first attempt to generalize this technique to manifold-valued images. Such images, for example images with phase or directional entries or with values in the manifold of symmetric positive definite matrices, are frequently encountered in real-world applications. Generalizing the normal law to manifolds is not canonical and different attempts have been considered. Here we focus on a straightforward intrinsic model and discuss the relation to other approaches for specific manifolds. We reinterpret the Bayesian approach of Lebrun et al. [41] in terms of minimum mean squared error estimation, which motivates our definition of a corresponding estimator on the manifold. With this estimator at hand we present a nonlocal patch-based method for the restoration of manifold-valued images. Various proof of concept examples demonstrate the potential of the proposed algorithm.

1. Introduction

In many situations where measurements are taken the obtained data are corrupted by noise, and typically one uses a stochastic model to describe the recorded data. If there are several, independent factors that may have an influence on the data acquisition, the central limit theorem suggests to model the noise as additive white Gaussian noise. This is also the standard noise model one encounters in image analysis, see, e.g., [31]. One might of course wonder whether this noise modeling is realistic and in fact, in many situations the image formation process already suggests a non-Gaussian model, e.g. Poisson noise in the case where images are obtained based on photon counting with a CCD device. But also in these cases, in order to benefit from the rich knowledge and all the appealing properties

*Department of Mathematics, Technische Universität Kaiserslautern, Paul-Ehrlich-Str. 31, 67663 Kaiserslautern, Germany, {friederike.laus, persch, steidl}@mathematik.uni-kl.de.

[†]CMLA – CNRS, ENS Cachan, 61 av. President Wilson, 94235 Cachan Cedex, France, nikolova@cmla.ens-cachan.fr

of the normal distribution, one often tries to transform the image in such a way that the assumption of Gaussian white noise is at least approximately fulfilled. For instance, for the Poisson noise this can be achieved by the so called Anscombe transform [4].

Much effort has been spent on the denoising of images corrupted with white Gaussian noise and a huge amount of methods have been proposed in the literature. Among others we mention variational models with total variation regularizers [60] and many extensions thereof, denoising based on sparse representations over learned dictionaries [26], nonlocal means [30, 63, 80, 77] and their generalizations [17, 23, 38, 63], the piecewise linear estimator from Gaussian mixture models (PLE, E-PLE) [80, 73] and SURE guided Gaussian mixture models [74], patch-ordering based wavelet methods [56], the expected patch log-likelihood (EPLL) algorithm [81] or better its multiscale variant [52], BM3D [21] and BM3D-SAPCA [22], and the nonlocal Bayes' algorithm of Lebrun et al. [40, 41]. The latter can be viewed as an optimized reinterpretation of the two step image denoising method (TSID) [64, 78] in a Bayesian framework. For a recent review of the denoising problem and the different denoising principles we refer to [42]. Currently, nonlocal patch-based methods achieve the best results and the quality of the denoised images has become excellent for moderate noise levels. Even more, based on experiments with a set of 20.000 images containing about 10^{10} patches the authors of [47] conjecture that for natural images, the recent patch-based denoising methods might already be close to optimality. Their conjecture points in the same direction as the paper of Chatterjee et al. [16], who raised the question „Is denoising dead?“.

The situation described above completely changes when dealing with manifold-valued images instead of real-valued ones, a situation which is frequently encountered in applications. For instance, images with values on the circle (periodic data) appear in interferometric synthetic aperture radar [13, 24], in applications involving the phase of Fourier transformed data [10], or when working with the hue-component of an image in the HSV color space. Spherical data play a role when dealing with 3D directional information [39, 70] or in the representation of a color image in the chromaticity-brightness (CB) color space [15]. SO(3)-valued data appear in electron backscattered tomography [8, 9]. Finally, to mention only a few examples, images with symmetric positive definite matrices as values are handled in DT-MRI imaging [18, 28, 69, 75, 77] or when covariance matrices are associated to image pixels [68]. Recently, some methods for the denoising of manifold-valued images have been suggested, among them variational approaches using embeddings in higher dimensional spaces [59] or based on (generalized) TV-regularization [7, 11, 46, 66, 76].

In this paper, we aim at generalizing the nonlocal patch-based denoising of Lebrun et al. [40, 41] to manifold-valued images. However, for general manifolds, already the question of how to define Gaussian white noise (or, more general, a normal distribution) is not canonically solved. Different approaches have been proposed in the literature, either by making use of characterizing properties of the real-valued normal distribution as for instance in [51, 53] or by restricting to particular manifolds such as spheres, see, e.g. [48], the simplex [49], or symmetric positive definite matrices [61]. In this paper, we adopt a simple model for a normal distribution and in particular for Gaussian white noise on a manifold and discuss its relationship to existing models. We review the minimum mean squared error estimator in the Euclidean setting, which coincides with those of the Bayesian approach in [41] under the normal distribution assumption. This motivates our definition of a corresponding estimator on the manifold and gives rise to a nonlocal patch-based method for

the restoration of manifold-valued images.

The outline of this paper is as follows: in Section 2 we reinterpret the nonlocal Bayes algorithm of Lebrun et al. [40, 41] in a minimum mean square error estimation setting. This review in the Euclidean setting is necessary to understand its generalization to manifold-valued images. In Section 3 we introduce the notation on manifolds. Then, in Section 4 we detail the nonlocal patch-based denoising algorithm for manifold valued images. This requires to precise what we mean by the normal law on the manifolds of interest. We discuss the relation between this model and other existing ones. In Section 5 we provide several numerical examples to demonstrate that our denoising approach is indeed computationally manageable. Examples, yet academical, for cyclic and directional data, and for images with values in the manifold of symmetric positive definite matrices show the potential of nonlocal techniques for manifold-valued images. Specific real-world applications are not within the scope of this paper. Finally, we draw conclusions and initiate further directions of research in Section 6.

2. Nonlocal Patch-Based Denoising of Real-Valued Images

In this section we consider the nonlocal Bayesian image denoising method of Lebrun et al. [40, 41]. In contrast to these authors we prefer to motivate the method by a minimum mean square estimation approach. One reason is that the best *linear* unbiased estimator in (6) has a similar form as the MMSE, but does not rely on the assumption that the random variables are jointly normally distributed. This leaves potential for future work, e.g. when extending the model to other distributions than the normal distribution.

2.1. Minimum Mean-Square Estimator

Let $(\Omega, \mathcal{A}, \mathbb{P})$ be a probability space and $X: \Omega \rightarrow \mathbb{R}^n$ and $Y: \Omega \rightarrow \mathbb{R}^n$ two random vectors. We wish to estimate X given Y , i.e., we seek an estimator $T: \mathbb{R}^n \rightarrow \mathbb{R}^n$ such that $\hat{X} = T(Y)$ approximates X . A common quality measure for this task is the *mean square error* $\mathbb{E} \|X - T(Y)\|_2^2$, which gives rise to the definition of the *minimum mean square estimator* (MMSE)

$$\begin{aligned} T_{\text{MMSE}}(Y) &= \arg \min_T \mathbb{E} \|X - T(Y)\|_2^2 \\ &= \arg \min_{Z \in \sigma(Y)} \mathbb{E} \|X - Z\|_2^2, \end{aligned}$$

where $\sigma(Y)$ denotes the σ -algebra generated by Y and $Z \in \sigma(Y)$ stands for all $\sigma(Y)$ -measurable random variables Z , see, e.g., [43]. Under weak additional regularity assumptions on the estimator T , the Lehmann-Scheffé theorem [44, 45] states that the general solution of the minimization problem is determined by

$$T_{\text{MMSE}}(Y) = \mathbb{E}(X|Y).$$

In general it is not possible to give an analytical expression of the MMSE. One exception constitutes of the normal distribution. Recall that a random vector X is normally distributed with mean $\mu \in \mathbb{R}^n$ and covariance matrix $\Sigma \in \mathbb{R}^{n \times n}$, $X \sim \mathcal{N}(\mu, \Sigma)$, if and only if

there exists a random vector $Z \in \mathbb{R}^l$, whose components are independent real-valued standard normally distributed random variables and a $p \times l$ matrix A , such that $X = AZ + \mu_X$, where l is the rank of the covariance matrix $\Sigma_X = AA^T$. If Σ_X has full rank, then the probability density function (pdf) of $X \sim \mathcal{N}(\mu, \Sigma)$ with respect to the Lebesgue measure is given by

$$p_X(x|\mu, \Sigma) = \frac{1}{(2\pi)^{\frac{n}{2}}} \frac{1}{|\Sigma|^{\frac{1}{2}}} e^{-\frac{1}{2}(x-\mu)^T \Sigma^{-1}(x-\mu)}, \quad (1)$$

where $|\Sigma|$ denotes the determinant of Σ . In view of the next section it is useful to recall some properties of the normal distribution.

Remark 2.1. (Properties of Gaussian distribution on \mathbb{R}^n)

- (i) *The Gaussian density function in (1) maximizes the entropy $H(X) := \mathbb{E}[-\log(p_X(X|\mu, \Sigma))]$ over all density functions on \mathbb{R}^n with fixed mean μ and covariance matrix Σ .*
- (ii) *Let $x_1, \dots, x_K \in \mathbb{R}^n$, $K \in \mathbb{N}$, be i.i.d. realizations of an absolutely continuous distribution having first and second moments, denoted by μ and Σ . Then the likelihood function reads as $L(\mu, \Sigma|x_1, \dots, x_K) = \prod_{k=1}^K p_X(x_k|\mu, \Sigma)$ and the maximum likelihood (ML) estimator is defined as*

$$\hat{\mu} := \arg \max_{\mu} L(\mu, \Sigma|x_1, \dots, x_K).$$

It holds that

$$\hat{\mu} = \frac{1}{K} \sum_{k=1}^K x_k = \arg \min_{x \in \mathbb{R}^n} \sum_{k=1}^K \|x - x_k\|_2^2 \quad (2)$$

if and only if the density function is of the form (1), see, e.g., [25, 65]. For the normal distribution the ML estimator of the covariance matrix reads as

$$\hat{\Sigma} = \frac{1}{K} \sum_{k=1}^K (x_k - \hat{\mu})(x_k - \hat{\mu})^T. \quad (3)$$

- (iii) *The density function of the standard normal distribution $\mathcal{N}(0, \sigma^2 I_n)$ with the $n \times n$ identity matrix I_n is the kernel of the heat equation.*

In order to compute the MMSE estimator for Gaussian random variables we need to determine the conditional distribution of X given Y . It is well known that, if $X \sim \mathcal{N}(\mu_X, \Sigma_X)$ and $Y \sim \mathcal{N}(\mu_Y, \Sigma_Y)$ are jointly normally distributed, i.e.,

$$\begin{pmatrix} X \\ Y \end{pmatrix} \sim \mathcal{N}\left(\begin{pmatrix} \mu_X \\ \mu_Y \end{pmatrix}, \begin{pmatrix} \Sigma_X & \Sigma_{XY} \\ \Sigma_{YX} & \Sigma_Y \end{pmatrix}\right),$$

then the conditional distribution of X given $Y = a$ is normally distributed as well and reads as

$$(X|Y = a) \sim \mathcal{N}(\mu_{X|Y}, \Sigma_{X|Y}),$$

where

$$\mu_{X|Y} = \mu_X + \Sigma_{XY}\Sigma_Y^{-1}(a - \mu_Y), \quad \Sigma_{X|Y} = \Sigma_X - \Sigma_{XY}\Sigma_Y^{-1}\Sigma_{YX}.$$

As a consequence we obtain for normally distributed random vectors the MMSE estimator

$$T_{\text{MMSE}}(Y) = \mathbb{E}(X|Y) = \mu_X + \Sigma_{XY}\Sigma_Y^{-1}(Y - \mu_Y). \quad (4)$$

In our situation (denoising) fits into the above framework if we set

$$Y = X + \eta, \quad X \sim \mathcal{N}(\mu_X, \Sigma_X), \quad \eta \sim \mathcal{N}(0, \sigma^2 I_n),$$

where we assume that X and η are independent and $\sigma^2 > 0$ is known. Then $\mu_X = \mu_Y$, and by the independence of X and η further $\Sigma_{XY} = \Sigma_X$ and

$$\Sigma_Y = \mathbb{E}((X + \eta - \mu_X)(X + \eta - \mu_X)^\top) = \Sigma_X + \sigma^2 I_n. \quad (5)$$

Now, the MMSE of X given Y in (4) becomes

$$\begin{aligned} T_{\text{MMSE}}(Y) &= \mu_X + \Sigma_X(\Sigma_X + \sigma^2 I_d)^{-1}(Y - \mu_X) \\ &= \mu_Y + (\Sigma_Y - \sigma^2 I_n)\Sigma_Y^{-1}(Y - \mu_Y). \end{aligned}$$

Two remarks may be useful to see the relation to other estimators.

Remark 2.2. (Relation between MMSE and BLUE)

The estimator of the general form

$$T_{\text{BLUE}}(Y) = \mathbb{E}(X) + \Sigma_{XY}\Sigma_Y^{-1}(Y - \mathbb{E}(Y)) \quad (6)$$

makes also sense for more general distributions. It is known as best linear unbiased estimator (BLUE), as it is an unbiased estimator which has minimum mean-square error among all affine estimators. For jointly normally distributed X and Y it coincides with T_{MMSE} .

Remark 2.3. (Relation between MMSE and MAP)

The MMSE can also be derived in a Bayesian framework under a Gaussian prior (see, e.g. [27]), which is detailed in the following. Let $Y = X + \eta$, $X \sim \mathcal{N}(\mu_X, \Sigma_X)$, $\eta \sim \mathcal{N}(0, \sigma^2 I_d)$, where X and η are independent. This implies $Y \sim \mathcal{N}(\mu_X, \Sigma_X + \sigma^2 I_d)$ and $(Y|X = x) \sim \mathcal{N}(x, \sigma^2 I_d)$, so that the respective densities are given by

$$p_Y(y|X = x) = \frac{1}{(2\pi\sigma^2)^{\frac{d}{2}}} e^{-\frac{1}{2\sigma^2}\|y-x\|_2^2}$$

and

$$p_X(x) = \frac{1}{(2\pi)^{\frac{d}{2}}} \frac{1}{|\Sigma_X|^{\frac{1}{2}}} e^{-\frac{1}{2}(x-\mu_X)^\top \Sigma_X^{-1}(x-\mu_X)}.$$

By Bayes' formula we have

$$p_X(x|Y = y) = \frac{p_Y(y|X = x)p_X(x)}{p_Y(y)} \propto p_Y(y|X = x)p_X(x),$$

and therewith, the maximum a posteriori (MAP) estimate reads as

$$\begin{aligned}\hat{x} &= \arg \max_x \{p_X(x|Y=y)\} = \arg \max_x \{p_Y(Y|X=x)p_X(x)\} \\ &= \arg \max_x \left\{ \log(p_Y(Y|X=x)) + \log(p_X(x)) \right\} \\ &= \arg \min_x \left\{ \frac{1}{2\sigma^2} \|x-y\|_2^2 + \frac{1}{2} (x-\mu_X)^T \Sigma_X^{-1} (x-\mu_X) \right\}.\end{aligned}$$

Setting the gradient to zero results in

$$(I_d + \sigma^2 \Sigma_X^{-1}) \hat{x} = \sigma^2 \Sigma_X^{-1} \mu_X + y.$$

Observing that $I_d + \sigma^2 \Sigma_X^{-1} = \Sigma_X^{-1} (\Sigma_X + \sigma^2 I_d)$ and $\sigma^2 (\Sigma_X + \sigma^2 I_d)^{-1} = I_d - \Sigma_X (\Sigma_X + \sigma^2 I_d)^{-1}$, we obtain finally

$$\begin{aligned}\hat{x} &= \sigma^2 (\Sigma_X + \sigma^2 I_d)^{-1} \mu_X + (\Sigma_X + \sigma^2 I_d)^{-1} \Sigma_X y \\ &= \mu_X + \Sigma_X (\Sigma_X + \sigma^2 I_d)^{-1} (y - \mu_X).\end{aligned}$$

In practical applications, the parameters μ_Y and Σ_Y are unknown and need to be estimated using realizations (observations) y_1, \dots, y_K of Y . Here we use the ML estimators given in (2) and (3). Note that the ML estimator for the covariance matrix is slightly biased. Instead we could also deal with an unbiased estimator by replacing the averaging factor by $\frac{1}{K-1}$. However, the numerical difference is negligible for large K .

Summarizing our findings, we obtain the following empirical estimator

$$\hat{T}_{\text{MMSE}}(y) = \hat{\mu}_Y + (\hat{\Sigma}_Y - \sigma^2 I_n) \hat{\Sigma}_Y^{-1} (y - \hat{\mu}_Y). \quad (7)$$

Remark 2.4 (Positive definiteness of the empirical covariance matrix). Equation (7) contains via (5) the hidden assumption that $\hat{\Sigma}_X = \hat{\Sigma}_Y - \sigma^2 I_n$. However, based on the empirical covariance matrix $\hat{\Sigma}_Y$ it is not necessarily ensured that $\hat{\Sigma}_Y - \sigma^2 I_n$ is positive semi-definite and thus a valid covariance matrix. There are different ways to overcome this problem, e.g. replacing negative eigenvalues by a small positive value as for instance proposed in [57], compare also the discussion in [40, Section 3.5] or [79, page 406]. In our numerical experiments we did not observe that this issue had negative impacts on the results.

2.2. Denoising Using the MMSE Approach

Next we describe how the results of the previous section can be used for image denoising. To this aim, let $x: \mathcal{G} \rightarrow \mathbb{R}$ be a discrete gray-value image, defined on a grid $\mathcal{G} = \{1, \dots, N_1\} \times \{1, \dots, N_2\}$. By a slight abuse of notation we also write $x \in \mathbb{R}^N$, where $N = N_1 N_2$ for the columnwise reshaped version of the image. It will be always clear from the context to which notation we refer. We assume that the image is corrupted with white Gaussian noise, i.e.,

$$y = x + \eta,$$

where η is now a realization of $\mathcal{N}(0, \sigma^2 I_N)$. Based on y we wish to reconstruct the original image x .

We use the fact that natural images are to some extent self-similar, i.e., small similar patches may be found several times in the image, and that for these patches locally a normality assumption holds approximately true, see, e.g. [81]. To formalize this idea, consider an $s \times s$ neighborhood (patch) y_i centered at $i = (i_1, i_2) \in \mathcal{G}$, where $s = 2\kappa + 1$, $\kappa \in \mathbb{N}$. After vectorization this corresponds to a realization of an n -dimensional normally distributed random vector $Y_i \sim \mathcal{N}(\mu_i, \Sigma_i)$, where $n = s^2$. This patch is referred to as a reference patch in the following. Similar patches are interpreted as other realizations of $\mathcal{N}(\mu_i, \Sigma_i)$. There are several strategies to define similar patches. Take for example, for a fixed $K \in \mathbb{N}$, the K nearest patches with respect to the Euclidean distance in a $w \times w$ search window around i , where $w = 2\nu + 1 \gg s$, $\nu \in \mathbb{N}$. Let $\mathcal{S}(i)$ denote the set of centers of patches similar to y_i . Then the estimates of the expectation value (2) and the covariance (3) become

$$\hat{\mu}_i = \frac{1}{K} \sum_{k \in \mathcal{S}(i)} y_k \quad \text{and} \quad \hat{\Sigma}_i = \frac{1}{K} \sum_{k \in \mathcal{S}(i)} (y_k - \hat{\mu}_i)(y_k - \hat{\mu}_i)^T.$$

The obtained estimates are then used to restore the reference patch and all its similar patches with (7) as:

$$\hat{y}_j = \hat{\mu}_i + (\hat{\Sigma}_i - \sigma^2 I_n) \hat{\Sigma}_i^{-1} (y_j - \hat{\mu}_i), \quad j \in \mathcal{S}(i). \quad (8)$$

Proceeding as above for all pixels $i \in \mathcal{G}$ yields a variable number of estimates for each pixel. Therewith, the final estimate at pixel i is obtained as an average over all patches containing the pixel i (aggregation). There are some fine-tuning steps that were partly also considered in [40, 41]. This is summarized in the following remark.

Remark 2.5. (Fine tuning steps)

- (i) Boundaries: *Special attention has to be paid to patches at the boundaries of an image. There are at least two possibilities: Either, one extends the image, e.g. by mirroring, or one considers only patches lying completely inside the image together with appropriately smaller search windows. To our opinion the second strategy is preferable since it does not introduce artificial information. However, it leads to less estimates at the boundaries of the image, but we observed that this does not yield visible artifacts in practice.*
- (ii) Flat areas: *Flat areas, where differences between patches are only caused by noise, require a special consideration, as it is very likely that the estimated covariance matrix will not have full rank. In this case, the patches are better denoised by only using their mean. Flat areas might be detected using the empirical variance of the patches, which is close to σ^2 .*
- (iii) Second step: *The similarity of patches and the covariance structure of the patches can be better estimated using the first step denoised image as an oracle image for a second step.*
- (iv) Acceleration: *To speed up the denoising procedure, each patch that has been used (and therefore denoised at least once) in a group of similar patches is not considered as reference patch anymore. Nevertheless, it may be denoised several times by being potentially chosen in other groups.*

Algorithm 1 Nonlocal MMSE Denoising Algorithm on \mathbb{R}^d , Step 1

Input: noisy image $y \in \mathbb{R}^{N,d}$, variance σ^2 of the noise

Output: first step denoised image \hat{y} and final image \tilde{y}

Parameters: s_1, s_2 sizes of patches, K_1, K_2 numbers of similar patches, γ homogeneous area parameter, w_1, w_2 sizes of search areas

Step 1:

for all patches $y_i \in \mathbb{R}^{s_1^2,d}$ of the noisy image y not considered before **do**

 Determine the set $\mathcal{S}_1(i)$ of centers of K_1 patches similar to y_i in a $w_1 \times w_1$ window around i

 Compute the empirical mean patch, $\hat{\mu}_i = (\hat{\mu}_{i,j})_{j=1}^{s_1^2}$,

$$\hat{\mu}_i = \frac{1}{K_1} \sum_{k \in \mathcal{S}_1(i)} y_k$$

Homogeneous area test: Compute the mean value $\hat{m}_i = \frac{1}{s_1^2} \sum_{j=1}^{s_1^2} \hat{\mu}_{i,j}$ and the empirical variance of the patches

$$\hat{\sigma}_i^2 = \frac{1}{dK_1s_1^2} \sum_{k \in \mathcal{S}_1(i)} (y_k - \mathbf{1}_{s_1^2} \otimes \hat{m}_i)^T (y_k - \mathbf{1}_{s_1^2} \otimes \hat{m}_i)$$

if $\hat{\sigma}_i^2 \leq \gamma\sigma^2$ **then**

 Compute the restored patches $\hat{y}_k = \mathbf{1}_{s_1^2} \otimes \hat{m}_i$, $k \in \mathcal{S}_1(i)$

else

 Compute the empirical covariance matrix

$$\hat{\Sigma}_i = \frac{1}{K_1} \sum_{k \in \mathcal{S}_1(i)} (y_k - \hat{\mu}_i)(y_k - \hat{\mu}_i)^T$$

 Compute the restored patches $\hat{y}_j = \hat{\mu}_i + (\hat{\Sigma}_i - \sigma^2 I_{s_1^2}) \hat{\Sigma}_i^{-1} (y_j - \hat{\mu}_i)$, $j \in \mathcal{S}_1(i)$

Aggregation: Obtain the first estimate \hat{y} at each pixel by computing the average over all restored patches containing the pixel

The whole denoising procedure is given in Algorithm 1. We would like to point out the differences between the two steps, which look at first glance very similar: Step 2 uses the denoised image from Step 1 in order to find similar patches and to estimate the covariance matrix, but reuses the original noisy image for the other computations, i.e, for the mean patch and the restored image.

Algorithm 1 Nonlocal MMSE Denoising Algorithm on \mathbb{R}^d , Step 2

Step 2:

for all patches y_i of the noisy image y not considered before **do**

Determine in a $w_2 \times w_2$ window around i the set $\mathcal{S}_2(i)$ of centers of K_2 patches which are similar to patch \hat{y}_i of the denoised image in Step 1.

Compute the empirical mean patch, $\hat{\mu}_i = (\hat{\mu}_{i,j})_{j=1}^{s_2^2}$,

$$\tilde{\mu}_i = \frac{1}{K_2} \sum_{k \in \mathcal{S}_2(i)} y_k$$

Homogeneous area test: Compute the mean value by $\tilde{m}_i = \frac{1}{s_2^2} \sum_{j=1}^{s_2^2} \tilde{\mu}_{i,j}$ and the empirical variance of the patches

$$\tilde{\sigma}_i^2 = \frac{1}{dK_2s_2^2} \sum_{k \in \mathcal{S}_2(i)} (y_k - \mathbf{1}_{s_2^2} \otimes \tilde{m}_i)^\top (y_k - \mathbf{1}_{s_2^2} \otimes \tilde{m}_i)$$

if $\tilde{\sigma}_i^2 \leq \gamma\sigma^2$ **then**

Compute the restored patches $\tilde{y}_j = \mathbf{1}_{s_2^2} \otimes \tilde{m}_i$, $j \in \mathcal{S}_2(i)$

else

Compute the empirical covariance matrix

$$\tilde{\Sigma}_i = \frac{1}{K_2} \sum_{k \in \mathcal{S}_2(i)} (\hat{y}_k - \tilde{\mu}_i)(\hat{y}_k - \tilde{\mu}_i)^\top + \sigma^2 I_{s_2^2}$$

Compute the restored patches $\tilde{y}_j = \tilde{\mu}_i + (\tilde{\Sigma}_i - \sigma^2 I_{s_2^2}) \tilde{\Sigma}_i^{-1} (y_j - \tilde{\mu}_i)$, $j \in \mathcal{S}_2(i)$

Aggregation: Obtain the final estimate \tilde{y} at each pixel by computing the average over all restored patches containing the pixel

The overall approach can be generalized to images with values in \mathbb{R}^d , $d > 1$, in a straightforward way, dealing now with n -dimensional random vectors, where $n = s^2d$. In particular, RGB-color images ($d = 3$) can be denoised in this way. At this point, considering the three color channels independently does usually not yield good results as there is a significant correlation between the red, the green, and the blue color channel. This correlation is correctly taken into account in the three-variate setting. As an alternative, Lebrun et al. [41] suggested to work in the so-called $Y_oU_oV_o$ color space [50], which is a variant of the YUV space where transform from the RGB space is orthogonal and thus does not change the noise statistics. This color system separates geometric from chromatic information and thereby decorrelates the color channels, so that treating them independently does not create noticeable color artifacts as it would be the case in the RGB space.

3. Random Points on Manifolds

Instead of \mathbb{R}^d -valued images we are now interested in images having values in a d -dimensional manifold M . We start by introducing the necessary notation in Riemannian manifolds. In our numerical examples we will deal with images having components on the d -sphere \mathbb{S}^d equipped with the Euclidean metric of the embedding spaces \mathbb{R}^{d+1} , $d = 1, 2$, and the manifold of positive definite $r \times r$ -matrices $\text{SPD}(r)$, $r = 2, 3$, with the affine invariant metric. For these manifolds the specific expressions of the following quantities are given in Appendix B. Further, we will consider the open probability simplex $\Delta_d \subset \mathbb{R}_{>0}^{d+1}$, $d = 1$, with the Rao-Fisher metric obtained from the categorical distribution and the hyperbolic manifold \mathbb{H}^d , $d = 2$, equipped with the Minkowski metric. Besides many textbooks on differential geometry the reader may have a look into Pennec’s paper [53] to get an overview. We adapted our notation to this paper.

Manifolds If not stated otherwise, let \mathcal{M} be a complete, connected n -dimensional Riemannian manifold. All of the previously mentioned manifolds are complete, except for the probability simplex. Observe that we will work with $s \times s$ patches of d -dimensional manifolds M such that we finally deal with product manifolds $\mathcal{M} = M^{s^2}$ of dimension $n = s^2d$ with the usual product metric. By $T_{\mathbf{x}}\mathcal{M}$ we denote the tangent space of \mathcal{M} at $\mathbf{x} \in \mathcal{M}$ and by $\langle \cdot, \cdot \rangle_{\mathbf{x}} : T_{\mathbf{x}}\mathcal{M} \times T_{\mathbf{x}}\mathcal{M} \rightarrow \mathbb{R}$ the Riemannian metric. Let $\gamma_{\mathbf{x},v}(t)$, $\mathbf{x} \in \mathcal{M}$, $v \in T_{\mathbf{x}}\mathcal{M}$, be the geodesic starting from $\gamma_{\mathbf{x},v}(0) = \mathbf{x}$ with $\dot{\gamma}_{\mathbf{x},v}(0) = v$. Since \mathcal{M} is complete, the exponential map $\exp_{\mathbf{x}} : T_{\mathbf{x}}\mathcal{M} \rightarrow \mathcal{M}$ with

$$\exp_{\mathbf{x}}(v) := \gamma_{\mathbf{x},v}(1)$$

is well-defined for every $\mathbf{x} \in \mathcal{M}$. The exponential map realizes a local diffeomorphism (exponential chart) from a “sufficiently small neighborhood” of the origin $0_{\mathbf{x}}$ of $T_{\mathbf{x}}\mathcal{M}$ into a neighborhood of $\mathbf{x} \in \mathcal{M}$. To precise how large this “small neighborhood” can be chosen, we follow the geodesic $\gamma_{\mathbf{x},v}$ from $t = 0$ to infinity. It is either minimizing all along or up to a finite time t_0 and not any longer afterwards. In the latter case, $\gamma_{\mathbf{x},v}(t_0)$ is called *cut point* and the corresponding tangent vector t_0v is called *tangential cut point*. The set of all cut points of all geodesics starting from \mathbf{x} is the *cut locus* $\mathcal{C}(\mathbf{x})$ and the set of corresponding vectors $\mathcal{C}_T(0_{\mathbf{x}})$ the *tangential cut locus*. Then the open domain $\mathcal{D}_T(0_{\mathbf{x}})$ around $0_{\mathbf{x}}$ bounded by the tangential cut locus is the maximal domain for which the exponential chart at \mathbf{x} is

injective. It is connected and star-shaped with respect to $0_{\mathbf{x}}$ and $\exp_{\mathbf{x}} \mathcal{D}_T(0_{\mathbf{x}}) = \mathcal{M} \setminus \mathcal{C}(\boldsymbol{\mu})$. This allows to define the inverse exponential map as

$$\log_{\mathbf{x}} := \exp_{\mathbf{x}}^{-1}: \mathcal{M} \setminus \mathcal{C}(\boldsymbol{\mu}) \rightarrow T_{\mathbf{x}}\mathcal{M}.$$

For the d -sphere \mathbb{S}^d the cut locus of \mathbf{x} is just its antipodal point $-\mathbf{x}$. Thus the tangential cut locus $\mathcal{D}_T(0_{\mathbf{x}})$ is the ball with radius π around $0_{\mathbf{x}}$ and $\mathcal{C}_T(0_{\mathbf{x}})$ its boundary. For Hadamard manifolds which are complete, simply-connected manifolds with non-positive sectional curvature [6], as SPD(r) or \mathbb{H}^d , we have that $\mathcal{D}_T(0_{\mathbf{x}}) = T_{\boldsymbol{\mu}}\mathcal{M}$.

The Riemannian metric yields a distance function $\text{dist}_{\mathcal{M}}: \mathcal{M} \times \mathcal{M} \rightarrow \mathbb{R}_{\geq 0}$ on the manifold by $\text{dist}_{\mathcal{M}}(\mathbf{x}, \mathbf{y}) = \langle \log_{\mathbf{x}}(\mathbf{y}), \log_{\mathbf{x}}(\mathbf{y}) \rangle_{\mathbf{x}}$ and a measure $d_{\mathcal{M}}(\mathbf{x})$ written in local coordinates $x = (x^1, \dots, x^n)$ by $d_{\mathcal{M}}(\mathbf{x}) = \sqrt{G(x)} dx$, where $G(x) := \langle \langle \frac{\partial}{\partial x^i}, \frac{\partial}{\partial x^j} \rangle_{\mathbf{x}} \rangle_{i,j=1}^n$ and $dx := dx^1 \dots dx^n$.

Random Points Let $(\Omega, \mathcal{A}, \mathbb{P})$ be a probability space and $\mathcal{B}(\mathcal{M})$ the Borel σ -algebra on \mathcal{M} (with respect to $\text{dist}_{\mathcal{M}}$). A measurable map $\mathbf{X}: \Omega \rightarrow \mathcal{M}$ is called a *random point* on \mathcal{M} . We consider only absolutely continuous random points \mathbf{X} with probability density $p_{\mathbf{X}}$, i.e., $\mathbb{P}(\mathbf{X} \in B) = \int_B p_{\mathbf{X}}(\mathbf{x}) d_{\mathcal{M}}(\mathbf{x})$ for all $B \in \mathcal{B}(\mathcal{M})$ and $\mathbb{P}(\mathbf{X} \in \mathcal{M}) = 1$. The *variance* of \mathbf{X} with respect to a given point \mathbf{y} is defined as

$$\sigma_{\mathbf{X}}^2(\mathbf{y}) := \mathbb{E}(\text{dist}_{\mathcal{M}}(\mathbf{X}, \mathbf{y})^2) = \int_{\mathcal{M}} \text{dist}_{\mathcal{M}}(\mathbf{x}, \mathbf{y})^2 p_{\mathbf{X}}(\mathbf{x}) d_{\mathcal{M}}(\mathbf{x}), \quad (9)$$

and local minimizers of $\mathbf{y} \mapsto \sigma_{\mathbf{X}}^2(\mathbf{y})$ are called *Riemannian centers of mass* [36]. For a discussion of the existence and uniqueness of global minimizers, known as *Fréchet expectation* or *means* $\mathbb{E}(\mathbf{X})$ of \mathbf{X} see, e.g., [1, 36, 37]. For Hadamard manifolds with curvature bounded from below the Riemannian center of mass exists and is unique. For the spheres \mathbb{S}^d , if the support of $p_{\mathbf{X}}$ is contained in a geodesic ball of radius $r < \pi/2$, then the Riemannian center of mass is unique within this ball and it is the global minimizer of (9). In the following we assume that the variance is finite and the cut locus has a probability measure zero at any point $\mathbf{y} \in \mathcal{M}$. Then a necessary condition for $\boldsymbol{\mu}$ to be a Riemannian center of mass is

$$\int_{\mathcal{M}} \log_{\boldsymbol{\mu}}(\mathbf{x}) d_{\mathcal{M}}(\mathbf{x}) = 0. \quad (10)$$

For Hadamard manifolds with curvature bounded from below this condition is also sufficient. Assuming that the mean $\boldsymbol{\mu} = \mathbb{E}(\mathbf{X})$ is known, we define the covariance matrix Σ of \mathbf{X} (with respect to $\boldsymbol{\mu}$) by

$$\Sigma = \mathbb{E}(\log_{\boldsymbol{\mu}}(\mathbf{X}) \log_{\boldsymbol{\mu}}(\mathbf{X})^{\text{T}}) = \int_{\mathcal{M}} \log_{\boldsymbol{\mu}}(\mathbf{x}) \log_{\boldsymbol{\mu}}(\mathbf{x})^{\text{T}} p_{\mathbf{X}}(\mathbf{x}) d_{\mathcal{M}}(\mathbf{x}). \quad (11)$$

In practice, typically $\mathbb{E}(\mathbf{X})$ and Σ are unknown and need to be estimated. Given observations $\mathbf{x}_1, \dots, \mathbf{x}_K \in \mathcal{M}$ of a random point \mathbf{X} , we estimate the mean point by

$$\hat{\boldsymbol{\mu}} \in \arg \min_{\mathbf{x} \in \mathcal{M}} \frac{1}{K} \sum_{k=1}^K \text{dist}_{\mathcal{M}}(\mathbf{x}, \mathbf{x}_k)^2, \quad (12)$$

which is according to [12] a consistent estimator of $\mathbb{E}(\mathbf{X})$ and can be computed by a gradient descent algorithm, see, e.g. [2]. An estimator for the covariance matrix reads as

$$\hat{\Sigma} = \frac{1}{K} \sum_{k=1}^K \log_{\hat{\mu}}(\mathbf{x}_k) \log_{\hat{\mu}}(\mathbf{x}_k)^{\text{T}}. \quad (13)$$

4. Nonlocal Patch-Based Denoising of Manifold-Valued Images

In this section we propose an NL-MMSE denoising algorithm for manifold-valued images. To this end, we have to specify what we mean by “normally distributed” random points on manifolds. In contrast to the vector space setting, there does not exist a canonical definition of a normally distributed random vector on a manifold since various properties characterizing the normal distribution on \mathbb{R}^n as those in Remark 2.1, cannot be generalized to the manifold setting in a straightforward way. Here we rely on a simple approach which transfers normally distributed zero mean random vectors on tangent spaces via the exponential map to the manifold. Based on this definition we will see how the NL-MMSE from Section 2 carries over to manifold-valued images.

4.1. Gaussian Random Points

In the following, we describe the Gaussian model used in this paper for Hadamard manifolds and spheres and discuss its relation to other models for small variances.

For each tangent space $T_{\mathbf{x}}\mathcal{M}$ with fixed orthonormal basis $\{e_{\mathbf{x},i}\}_{i=1}^n$ we can identify the element $\sum_{i=1}^n x^i e_{\mathbf{x},i} \in T_{\mathbf{x}}\mathcal{M}$ with the local coordinate vector $x = (x^i)_{i=1}^n \in \mathbb{R}^n$, which establishes an isometry between $T_{\mathbf{x}}\mathcal{M}$ and \mathbb{R}^n . Note that also the expressions in (11) and (13) are basis dependent, but assuming a fixed basis the relation skipped for simplicity of notation. Now, let $\mu \in \mathcal{M}$ and let $h: \mathbb{R}^n \rightarrow T_{\mu}\mathcal{M}$ be the linear isometric mapping

$$h(x) := \sum_{i=1}^n x^i e_{\mu,i} \in T_{\mu}\mathcal{M}. \quad (14)$$

Let $\mathcal{D}_{\mu} := h^{-1}(\mathcal{D}_T(0_{\mu})) \subseteq \mathbb{R}^n$. Since \exp_{μ} is continuous, we have for any $B \in \mathcal{B}(\mathcal{M})$ that $B_n := h^{-1}(\log_{\mu}(B)) \subseteq \mathcal{D}_{\mu}$ is a Borel set and for any integrable function F it holds

$$\int_B F(\mathbf{x}) \, d_{\mathcal{M}}(\mathbf{x}) = \int_{B_n} F(\exp_{\mu}(h(x))) |G(x)|^{\frac{1}{2}} \, dx,$$

where $G(x) = (\langle d(\exp_{\mu})_{h(x)}[e_{\mu,i}], d(\exp_{\mu})_{h(x)}[e_{\mu,j}] \rangle)_{i,j=1}^n$. Conversely, for any Borel set $B_n \subseteq \mathcal{D}_{\mu}$ and any integrable function f we see that $B := \exp_{\mu}(h(B_n)) \in \mathcal{B}(\mathcal{M})$ and

$$\int_{B_n} f(x) \, dx = \int_B f(h^{-1}(\log_{\mu}(x))) |\tilde{G}(\mathbf{x})|^{\frac{1}{2}} \, d_{\mathcal{M}}(\mathbf{x}), \quad (15)$$

where $\tilde{G}(\mathbf{x}) = (\langle d(\log_{\boldsymbol{\mu}})_{\mathbf{x}}[e_{\mathbf{x},i}], d(\log_{\boldsymbol{\mu}})_{\mathbf{x}}[e_{\mathbf{x},j}] \rangle_{\boldsymbol{\mu}})_{i,j=1}^n$. If $Z \sim \mathcal{N}(0, I_n)$ is standard normally distributed on \mathbb{R}^n with pdf p_Z , then

$$\mathbf{Z} := \exp_{\boldsymbol{\mu}}(h(Z)) \quad (16)$$

is a random point on \mathcal{M} . For Hadamard manifolds, we have $D_{\boldsymbol{\mu}} = \mathbb{R}^n$ so that for $\mathbf{x} := \exp_{\boldsymbol{\mu}}(h(x))$,

$$\|x\|_2^2 = \langle h(x), h(x) \rangle_{\boldsymbol{\mu}} = \langle \log_{\boldsymbol{\mu}}(\mathbf{x}), \log_{\boldsymbol{\mu}}(\mathbf{x}) \rangle_{\boldsymbol{\mu}} = \text{dist}_{\mathcal{M}}(\boldsymbol{\mu}, \mathbf{x})^2.$$

Thus, \mathbf{Z} has the pdf

$$\begin{aligned} p_{\mathbf{Z}}(\mathbf{z}) &= p_Z(h^{-1}(\log_{\boldsymbol{\mu}}(\mathbf{z}))) |\tilde{G}(\mathbf{z})|^{\frac{1}{2}} \\ &= \frac{1}{(2\pi)^{n/2}} e^{-\frac{1}{2} \text{dist}_{\mathcal{M}}(\boldsymbol{\mu}, \mathbf{z})^2} |\tilde{G}(\mathbf{z})|^{\frac{1}{2}}. \end{aligned} \quad (17)$$

Note that by incorporating the factor $|\tilde{G}(\mathbf{z})|^{\frac{1}{2}}$ into the density function we avoid problems as discussed in [35]. By construction and (10) it follows directly that the mean of \mathbf{Z} is $\boldsymbol{\mu}$ and the covariance (11) is I_n . We consider \mathbf{Z} as normally distributed on \mathcal{M} and write $\mathbf{Z} \sim \mathcal{N}_{\mathcal{M}}(\boldsymbol{\mu}, I_n)$. In other words, \mathbf{Z} is normally distributed on \mathcal{M} with mean $\boldsymbol{\mu}$ and covariance I_n if $Z := h^{-1}(\log_{\boldsymbol{\mu}}(\mathbf{Z}))$ is standard normally distributed on \mathbb{R}^n .

If $D_{\boldsymbol{\mu}} \neq \mathbb{R}^n$ as it is the case for d -spheres, we assume that up to a set of Lebesgue measure zero $\mathbb{R}^n = \bigcup_{j \in \mathcal{J}} \mathcal{D}_{\boldsymbol{\mu},j}$, where $\mathcal{J} \subseteq \mathbb{Z}$ is an index set and $\mathcal{D}_{\boldsymbol{\mu},0} := \mathcal{D}_{\boldsymbol{\mu}}$. Further, we suppose that there are diffeomorphisms $\varphi_j: \mathcal{D}_{\boldsymbol{\mu},j} \rightarrow \mathcal{D}_{\boldsymbol{\mu}}$ such that for $x \in \mathcal{D}_{\boldsymbol{\mu},j}$ it holds $\exp_{\boldsymbol{\mu}}(h(x)) = \exp_{\boldsymbol{\mu}}((h \circ \varphi_j)(x))$. Then, in order to obtain the pdf of \mathbf{Z} in (16), we have to replace p_Z in (17) by the wrapped function

$$\tilde{p}_Z(z) := \frac{1}{(2\pi)^{n/2}} \sum_{j \in \mathcal{J}} e^{-\frac{1}{2} \|\varphi_j^{-1}(z)\|_2^2} |\text{d}\varphi_j^{-1}(z)|, \quad z \in \mathcal{D}_{\boldsymbol{\mu}}. \quad (18)$$

Now, we follow the same lines as in the Euclidean setting and agree that \mathbf{X} is normally distributed with mean $\boldsymbol{\mu}$ and positive definite covariance $\Sigma = AA^T$ if $X = h^{-1}(\log_{\boldsymbol{\mu}}(\mathbf{X})) = AZ \sim \mathcal{N}(0, \Sigma)$, respectively,

$$\mathbf{X} := \exp_{\boldsymbol{\mu}}(h(X)), \quad X \sim \mathcal{N}(0, \Sigma), \quad (19)$$

and write $\mathbf{X} \sim \mathcal{N}_{\mathcal{M}}(\boldsymbol{\mu}, \Sigma)$.

The following proposition shows how the pdf of a normally distributed random point (16) looks for various one-dimensional manifolds.

Proposition 4.1. *The pdf of a random point $\mathbf{X} \sim \mathcal{N}_{\mathcal{M}}(\boldsymbol{\mu}, \sigma^2 I_n)$ is given by*

(i) *the log-normal distribution for $\mathcal{M} = \mathbb{R}_{>0} = \text{SPD}(1)$,*

$$p_{\mathbf{X}}(\mathbf{x}) = \frac{1}{\sqrt{2\pi\sigma^2}} e^{-\frac{1}{2\sigma^2} (\ln(\mathbf{x}) - \ln(\boldsymbol{\mu}))^2}$$

with respect to the measure $\text{d}_{\mathbb{R}_{>0}}(\mathbf{x}) = \frac{1}{\mathbf{x}} \text{d}\mathbf{x}$ on $\mathbb{R}_{>0}$;

(ii) the 2π -wrapped Gaussian distribution for $\mathcal{M} = \mathbb{S}^1$,

$$p_{\mathbf{X}}(\mathbf{x}(t)) = \frac{1}{\sqrt{2\pi\sigma^2}} \sum_{j \in \mathbb{Z}} e^{-\frac{1}{2\sigma^2}(t-t_\mu+2j\pi)^2}$$

with respect to the parameterization

$\boldsymbol{\mu} := (\cos(t_\mu), \sin(t_\mu))^T$ and the Lebesgue measure dt ;

(iii) the 2π -wrapped, even shifted Gaussian distribution for $\mathcal{M} = \Delta_1$,

$$p_{\mathbf{X}}(\mathbf{x}(t)) = \frac{1}{\sqrt{2\pi\sigma^2}} \sum_{j \in \mathbb{Z}} \left(e^{-\frac{1}{2\sigma^2}(t+t_\mu+2j\pi)^2} + e^{-\frac{1}{2\sigma^2}(t-t_\mu+2j\pi)^2} \right)$$

with respect to the parameterization $\mathbf{x}(t) = \frac{1}{2}(1 + \cos(t), 1 - \cos(t))^T$, $t \in (0, \pi)$,
 $\boldsymbol{\mu} = \frac{1}{2}(1 + \cos(t_\mu), 1 - \cos(t_\mu))^T$ and Lebesgue measure dt .

The proof of the proposition is given in the Appendix A.

The above definition (19) of normally distributed random points has the advantage that it adopts the affine invariance of the Gaussian distribution known from the Euclidean setting via the tangent space. Moreover, it is easy to sample from the distribution.

Remark 4.2 (Sampling from $\mathcal{N}_{\mathcal{M}}(\boldsymbol{\mu}, \sigma^2 I_n)$). *Sampling of a $\mathcal{N}_{\mathcal{M}}(\boldsymbol{\mu}, \sigma^2 I_n)$ distributed random variable can be performed as follows: i) sample from $\mathcal{N}(0, \sigma^2 I_n)$ in \mathbb{R}^n , ii) apply h which by (14) requires only the knowledge of an orthogonal basis in $T_{\boldsymbol{\mu}}\mathcal{M}$, and iii) map the result by $\exp_{\boldsymbol{\mu}}$ to \mathcal{M} .*

For the one-dimensional manifolds in Proposition 4.1, the pdfs in (i) - (iii) are the kernels of the heat equations with the corresponding Laplace-Beltrami operators. This is in general not true for higher dimensions [33]. However, numerical experiments show that samples from the Gauss-Weierstrass kernel on \mathbb{S}^2 [29, p. 112] and from the heat kernel on $\text{SPD}(r)$ [67, p. 107] are very similar. For kernel density estimations on special Hadamard spaces we refer also to [19] and for kernels in connection with dithering on the sphere we refer to [32].

Neither the maximizing entropy nor the ML estimation property from Remark 2.1 generalize to the above setting. In [53] Pennec showed that under certain conditions on $\mathcal{D}_T(0_{\boldsymbol{\mu}})$ the pdf of a random point on \mathcal{M} that maximizes the entropy given prescribed mean value $\boldsymbol{\mu}$ and covariance Σ is of the form $\frac{1}{\psi} e^{-\frac{1}{2}(\log_{\boldsymbol{\mu}}(\mathbf{x}))^T \Sigma (\log_{\boldsymbol{\mu}}(\mathbf{x}))}$ with normalization constant ψ . Said and co-workers made use of the ML-estimator property in order to generalize the (isotropic) normal distribution to $\mathcal{M} = \text{SPD}(r)$ in [61] and to symmetric spaces of non-compact type in [62]. They proposed the following density function for a normal distribution with mean $\boldsymbol{\mu}$ and covariance $\sigma^2 I_n$:

$$p_{\mathbf{X}}(\mathbf{x}) = \frac{1}{\psi(\sigma)} e^{-\frac{1}{2\sigma^2} \text{dist}_{\mathcal{M}}(\boldsymbol{\mu}, \mathbf{x})^2}. \quad (20)$$

For the concrete definition of ψ and the noise simulation according to this model in the case of $\mathcal{M} = \text{SPD}(r)$ see [61] and the Appendix C. For $n = 1$ the models coincide by Proposition 4.1. For this distribution it is clear that the Riemannian center of mass is given by $\boldsymbol{\mu}$ and that the ML estimator for $\boldsymbol{\mu}$ is the empirical Karcher mean. Figure 1, left shows a 100×100 image of realizations of normally distributed noise on $\text{SPD}(2)$ by our

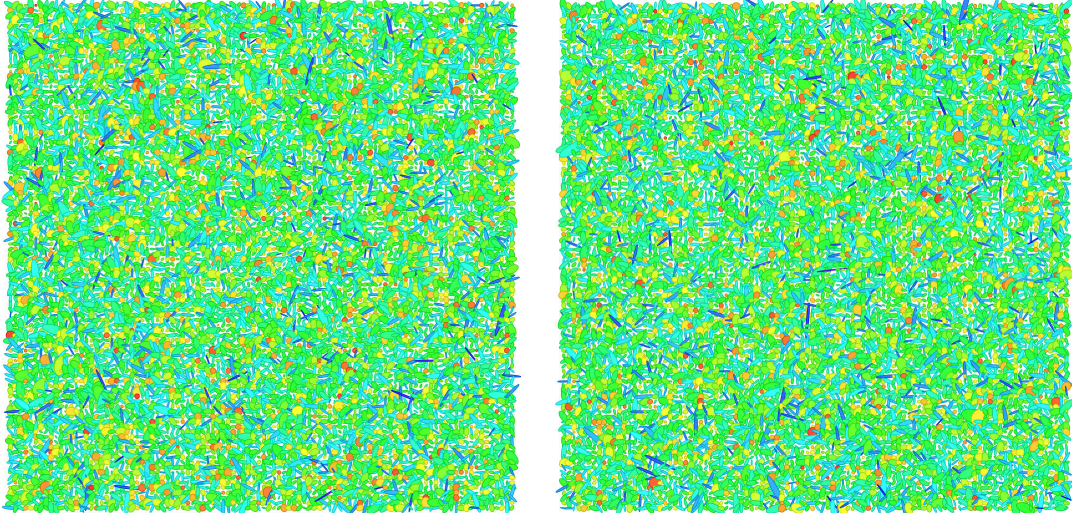


Figure 1. Sampling with respect to our noise model and that of Said et al. [61] for 100×100 samples and $\mathcal{N}(I_2, \sigma^2 I_2)$ with $\sigma = 0.5$.

model $\mathcal{N}(I_2, \sigma^2 I_2)$, where $\sigma = 0.5$. For comparison, in Figure 1, right the same is shown for realizations of $\mathcal{N}_{Said}(I_d, \sigma^2 I_d)$, also for $\sigma = 0.5$. The noise looks visually very similar, which is also confirmed by Table 1. The first two rows of Table 1 present the estimated mean $\boldsymbol{\mu}$ based on (12), the covariance matrix Σ based on (13) and the estimated standard deviation σ for our noise model and those of Said et al..

	$\boldsymbol{\mu}$	σ	Σ
\mathcal{N}_{Said}	$\begin{pmatrix} 0.9960 & 0.0044 \\ 0.0044 & 0.9944 \end{pmatrix}$	0.5051	$\begin{pmatrix} 0.2513 & 0.0025 & -0.0044 \\ 0.0025 & 0.2533 & -0.0017 \\ -0.0044 & -0.0017 & 0.2608 \end{pmatrix}$
\mathcal{N}	$\begin{pmatrix} 0.9980 & 0.0036 \\ 0.0036 & 0.9943 \end{pmatrix}$	0.5026	$\begin{pmatrix} 0.2567 & 0.0017 & 0.0001 \\ 0.0017 & 0.2487 & -0.0008 \\ 0.0001 & -0.0008 & 0.2523 \end{pmatrix}$

Table 1. Estimated parameters for the noise in Figure 1.

Below we give an example for the above pdf (20) and those in (17) for the manifold $\mathcal{M} = \mathbb{H}^2$.

Example 4.3. Let $\mathbb{H}^2 := \{\mathbf{x} \in \mathbb{R}^3 : x_1^2 + x_2^2 - x_3^2 = -1, x_3 > 0\}$ be the hyperbolic manifold equipped with the Minkowski metric $\langle \mathbf{x}, \mathbf{y} \rangle_{\mathbb{H}^2} := x_1 y_1 + x_2 y_2 - x_3 y_3$. The distance reads as $\text{dist}_{\mathbb{H}^2}(\mathbf{x}, \mathbf{y}) = \text{arcosh}(-\langle \mathbf{x}, \mathbf{y} \rangle_{\mathbb{H}^2})$ and

$$\exp_{\mathbf{x}}(v) = \cosh\left(\sqrt{\langle v, v \rangle_{\mathbb{H}^2}}\right) \mathbf{x} + \sinh\left(\sqrt{\langle v, v \rangle_{\mathbb{H}^2}}\right) \frac{v}{\sqrt{\langle v, v \rangle_{\mathbb{H}^2}}},$$

$$\log_{\mathbf{x}}(\mathbf{y}) = \frac{\text{arcosh}(-\langle \mathbf{x}, \mathbf{y} \rangle_{\mathbb{H}^2})}{(\langle \mathbf{x}, \mathbf{y} \rangle_{\mathbb{H}^2}^2 - 1)^{\frac{1}{2}}} (\mathbf{x} + \langle \mathbf{x}, \mathbf{y} \rangle_{\mathbb{H}^2} \mathbf{x}).$$

We parametrize $\mathbf{x} \in \mathbb{H}^2$ as

$$\mathbf{x}(\alpha, r) = \begin{pmatrix} \cos(\alpha) \sinh(r) \\ \sin(\alpha) \sinh(r) \\ \cosh(r) \end{pmatrix}, \quad \alpha \in [0, 2\pi), \quad r \in [0, \infty).$$

First, we compute the pdf (17) of an $\mathcal{N}_{\mathbb{H}^2}(\boldsymbol{\mu}, \sigma^2 I_2)$ distributed random point, where $\boldsymbol{\mu} := (0, 0, 1)^\top$. We obtain $\text{dist}_{\mathbb{H}^2}(\boldsymbol{\mu}, \mathbf{x}) = r$ and $\{e_{\boldsymbol{\mu},1} = (1, 0, 0)^\top, e_{\boldsymbol{\mu},2} = (0, 1, 0)^\top\}$ and for the other points ($r \neq 0$)

$$e_{\mathbf{x},1} := \frac{1}{\sinh(r)} \frac{\partial}{\partial \alpha} \mathbf{x}(\alpha, r) = \begin{pmatrix} -\sin(\alpha) \\ \cos(\alpha) \\ 0 \end{pmatrix}, \quad e_{\mathbf{x},2} := \frac{\partial}{\partial r} \mathbf{x}(\alpha, r) = \begin{pmatrix} \cos(\alpha) \cosh(r) \\ \sin(\alpha) \cosh(r) \\ \sinh(r) \end{pmatrix}.$$

Then the measure on \mathbb{H}^2 reads $d_{\mathbb{H}^2}(\mathbf{x}) = \sinh(r) d\alpha dr$. Straightforward computation gives

$$d(\log_{\boldsymbol{\mu}})_{\mathbf{x}}[e_{\mathbf{x},1}] = \frac{r}{\sinh(r)} \begin{pmatrix} -\sin(\alpha) \\ \cos(\alpha) \\ 0 \end{pmatrix}, \quad d(\log_{\boldsymbol{\mu}})_{\mathbf{x}}[e_{\mathbf{x},2}] = \begin{pmatrix} \cos(\alpha) \\ \sin(\alpha) \\ 0 \end{pmatrix}$$

so that $|\tilde{G}(\mathbf{x})|^{\frac{1}{2}} = r/\sinh(r)$. Consequently, the density (17) is

$$p_{\mathbf{X}}(\mathbf{x}(\alpha, r)) = \frac{1}{2\pi\sigma^2} e^{-\frac{r^2}{2\sigma^2}} \frac{r}{\sinh(r)}.$$

In contrast, the entropy minimizing pdf (20) is given by

$$p_{\mathbf{X}}(\mathbf{x}(\alpha, r)) = \frac{1}{\psi} e^{-\frac{r^2}{2\sigma^2}}, \quad \psi := 2\pi \int_0^\infty e^{-\frac{r^2}{2\sigma^2}} \sinh(r) dr = 2\pi\sigma e^{\frac{\sigma^2}{2}} \int_0^\sigma e^{-\frac{t^2}{2}} dt.$$

Besides the kernels of the heat equation, the von Mises-Fisher distribution is frequently considered as ‘‘spherical normal distribution’’ on \mathbb{S}^d . We briefly comment on this distribution.

Remark 4.4 (Fisher-Mises distribution on \mathbb{S}^d). For \mathbb{S}^1 it is well-known that the wrapped Gaussian distribution is closely related to the von Mises distribution $M(\boldsymbol{\mu}, \kappa)$ [34, 71, 72] whose density function reads as

$$p_{\text{MF}}(\mathbf{x}|\boldsymbol{\mu}, \kappa) = \frac{1}{2\pi I_0(\kappa)} e^{\kappa \cos(\mathbf{x} - \boldsymbol{\mu})}, \quad \mathbf{x} \in [-\pi, \pi),$$

where I_n denotes is the modified Bessel function of first kind and order n . The parameter $\boldsymbol{\mu}$ is referred to as mean direction, $\kappa > 0$ is the concentration parameter. The von Mises distribution is the distribution that maximizes the entropy under the constraint that the real and imaginary parts of the first circular moment (or, equivalently, the circular mean and circular variance) are specified. The maximum likelihood characterization is analogously to the one given in Remark 2.1, where the sample mean is replaced by the sample mean direction. A good matching between the pdfs of the wrapped Gaussian and those of the von Mises for high concentration (i.e. large κ respective small σ^2) can be found by taking the

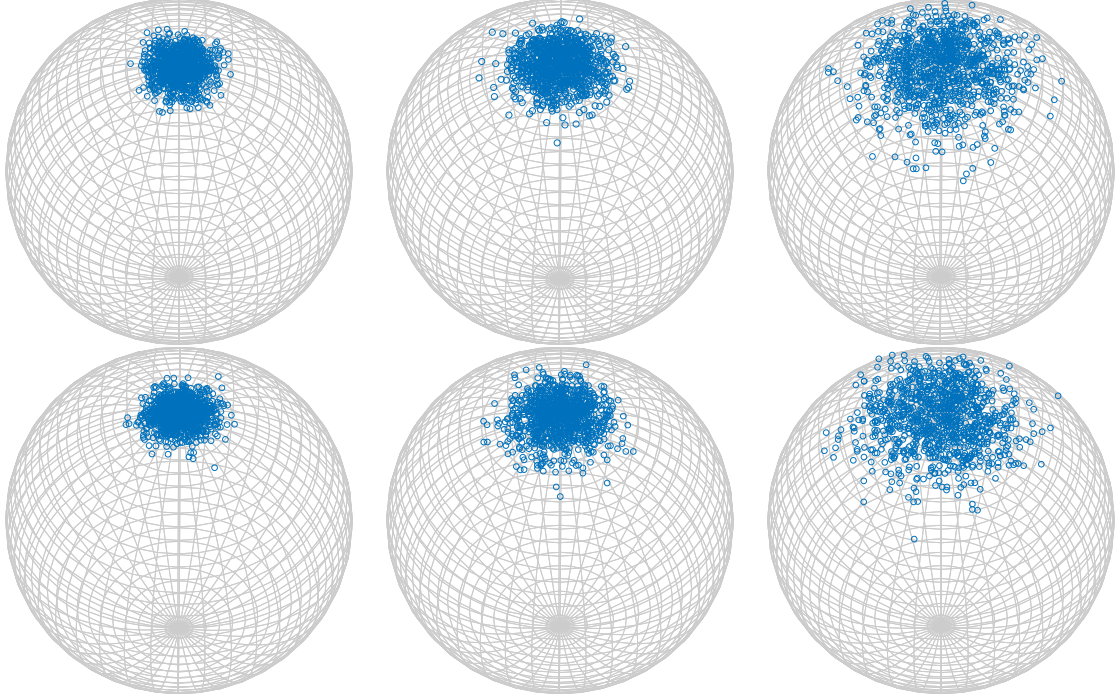


Figure 2. 1000 samples of Gaussian noise on \mathbb{S}^2 for $\boldsymbol{\mu} = (0, 0, 1)$ and $\sigma \in \left\{ \frac{1}{\sqrt{100}}, \frac{1}{\sqrt{50}}, \frac{1}{\sqrt{20}} \right\}$ (top, from left to right) and of the von Mises-Fisher distribution on \mathbb{S}^2 for $\boldsymbol{\mu} = (0, 0, 1)$ and $\kappa \in \{100, 50, 20\}$ (bottom, from left to right).

same center $\boldsymbol{\mu}$ and $\sigma^2 = -2 \log(A(\kappa))$ with $A(\kappa) = \frac{I_1(\kappa)}{I_0(\kappa)}$, see [48].

The von Mises distribution on \mathbb{S}^1 can be generalized to \mathbb{S}^d , leading to the von Mises-Fisher distribution given by

$$p_{\text{MF}}(\mathbf{x}|\boldsymbol{\mu}, \kappa) = \left(\frac{\kappa}{2}\right)^{\frac{d-1}{2}} \frac{1}{\Gamma\left(\frac{d+1}{2}\right) I_{\frac{d-1}{2}}(\kappa)} e^{\kappa \boldsymbol{\mu}^T \mathbf{x}},$$

where $\kappa > 0$, $\|\boldsymbol{\mu}\| = 1$ and Γ denotes the gamma function. For $d = 2$, the von Mises-Fisher distribution is also known as Fisher distribution and the pdf simplifies to

$$p_{\text{MF}}(\mathbf{x}|\boldsymbol{\mu}, \kappa) = \frac{\kappa}{\sinh(\kappa)} e^{\kappa \boldsymbol{\mu}^T \mathbf{x}}.$$

In Figure 2 we compare samples of our Gaussian noise model $\mathcal{N}(0, \sigma^2)$ with the von Mises-Fisher distribution $M(\boldsymbol{\mu}, \kappa)$ on \mathbb{S}^2 for $\boldsymbol{\mu} = (0, 0, 1)$ and $\sigma^2 = \frac{1}{\kappa}$.

4.2. NL-MMSE on Manifold-Valued Images

Assume that $\mathbf{Y} = \exp_{\boldsymbol{\mu}}(Y)$ is a random point on \mathcal{M} arising from a normally distributed random point $\mathbf{X} = \exp_{\boldsymbol{\mu}}(X) \sim \mathcal{N}_{\mathcal{M}}(\boldsymbol{\mu}, \Sigma)$ in the sense

$$Y = X + \eta, \quad X \sim \mathcal{N}(0_{\boldsymbol{\mu}}, \Sigma_X), \quad \eta \sim \mathcal{N}(0, \sigma^2 I_n),$$

where by slight abuse of notation we write $\exp_{\boldsymbol{\mu}}$ and $\log_{\boldsymbol{\mu}}$ instead of $\exp_{\boldsymbol{\mu}} \circ h$ and $h^{-1} \circ \log_{\boldsymbol{\mu}}$, respectively, as also done in Subsection 4.1. In the following we propose an estimator for \mathbf{X} based on $\mathbf{Y} = \exp_{\boldsymbol{\mu}}(Y)$, which arises from a two-step estimation procedure and is motivated by the Euclidean MMSE described in Section 2.1. In order to avoid technical difficulties we restrict our attention to Hadamard manifolds \mathcal{M} such that the exponential and logarithmic map are globally defined and the Riemannian center of mass exists and is uniquely determined.

In the first step, we estimate the mean $\boldsymbol{\mu} = \mathbb{E}(\mathbf{X})$ as

$$\boldsymbol{\mu} = \arg \min_{\mathbf{Z} \in \sigma(\{\emptyset, \Omega\})} \mathbb{E}[\text{dist}_{\mathcal{M}}(\mathbf{X}, \mathbf{Z})^2]. \quad (21)$$

Note that this corresponds to the definition given in (9), since those random variables \mathbf{Z} that are measurable with respect to the trivial σ -algebra $\{\emptyset, \Omega\}$ are exactly the constant random variables. By construction we have $\mathbb{E}(\mathbf{X}) = \mathbb{E}(\mathbf{Y})$. Once $\boldsymbol{\mu}$ is known, we estimate covariance matrix of X by

$$\begin{aligned} T_{\text{MMSE}}(\mathbf{Y}) &= \arg \min_{\log_{\boldsymbol{\mu}}(\mathbf{Z}) \in \sigma(\log_{\boldsymbol{\mu}}(\mathbf{Y}))} \mathbb{E}[\|\log_{\boldsymbol{\mu}}(\mathbf{X}) - \log_{\boldsymbol{\mu}}(\mathbf{Z})\|_2^2] \\ &= \arg \min_{Z \in \sigma(Y)} \mathbb{E}[\|X - Z\|_2^2] = \mathbb{E}(X|Y). \end{aligned} \quad (22)$$

In our specific Gaussian noise setting we are now in the same situation as described after Remark 2.1, so that by combining (21) and (22) we finally arrive at the estimator

$$T(\mathbf{Y}) = \exp_{\boldsymbol{\mu}}((\Sigma_Y - \sigma^2 I_n) \Sigma_Y^{-1} \log_{\boldsymbol{\mu}}(\mathbf{Y})).$$

Next, we describe how to estimate $\boldsymbol{\mu}$ and Σ_Y based on samples. To this aim, let $x: \mathcal{G} \rightarrow M$ be a discrete image defined on a grid $\mathcal{G} = \{1, \dots, N_1\} \times \{1, \dots, N_2\}$ with values in a d -dimensional manifold M . As for real-valued images, we consider small $s \times s$ image patches centered at $i = (i_1, i_2) \in \mathcal{G}$. We assume that the patch \mathbf{y}_i corresponds to a realization of a normally distributed random point $\mathbf{Y}_i \sim \mathcal{N}_{\mathcal{M}}(\boldsymbol{\mu}_i, \Sigma_i)$ on \mathcal{M} , where $\mathcal{M} = M^{s^2}$ is the product manifold of dimension $n = s^2 d$ equipped with the distance $\text{dist}_{\mathcal{M}}^2(\mathbf{x}, \mathbf{y}) = \sum_{j=1}^{s^2} \text{dist}_M(\mathbf{x}_j, \mathbf{y}_j)^2$. We fix $K \in \mathbb{N}$ and take the K nearest patches with respect to $\text{dist}_{\mathcal{M}}$ in a $w \times w$ search window around i . These patches are interpreted as other realizations of the same random point. Let $\mathcal{S}(i)$ denote the set of centers of the patches similar to \mathbf{y}_i . Then the empirical estimates for the mean and the covariance in (12), respective (13) read as

$$\hat{\boldsymbol{\mu}}_i \in \arg \min_{\boldsymbol{\mu} \in \mathcal{M}} \sum_{j \in \mathcal{S}(i)} \text{dist}_{\mathcal{M}}(\boldsymbol{\mu}, \mathbf{y}_j)^2, \quad \hat{\Sigma}_i = \frac{1}{K} \sum_{j \in \mathcal{S}(i)} \log_{\hat{\boldsymbol{\mu}}_i}(\mathbf{y}_j) \log_{\hat{\boldsymbol{\mu}}_i}(\mathbf{y}_j)^{\text{T}},$$

and are used to restore the reference patch and all its similar patches by

$$\hat{\mathbf{y}}_j = \exp_{\hat{\boldsymbol{\mu}}_i}((\hat{\Sigma}_i - \sigma^2 I_n) \hat{\Sigma}_i^{-1} (\log_{\hat{\boldsymbol{\mu}}_i}(\mathbf{y}_j))), \quad j \in \mathcal{S}(i). \quad (23)$$

This can be considered as the manifold counterpart to (8).

With slight modifications the fine-tuning details listed in Remark 2.5 can be generalized to manifolds. The treatment of patches at the boundaries, the acceleration and the second step are analogously as in the real-valued case, only for flat areas and the aggregation step one has to replace the empirical variance respective the mean by their manifold counterparts. The two steps of the algorithm are summarized in Algorithm 2.

Algorithm 2 Nonlocal MMSE Denoising Algorithm on M , Step 1

Input: noisy image $\mathbf{y} \in M^N$, variance σ^2 of noise

Output: first step denoised image $\hat{\mathbf{y}}$ and final image $\tilde{\mathbf{y}}$

Parameters: s_1, s_2 sizes of patches, K_1, K_2 numbers of similar patches, γ homogeneous area parameter, w_1, w_2 sizes of search area

Step 1:

Set $\mathcal{M} = M^{s_1^2}$

for all patches \mathbf{y}_i of the noisy image \mathbf{y} not considered before **do**

Determine the set $\mathcal{S}_1(i)$ of centers of K_1 patches similar to \mathbf{y}_i in a $w_1 \times w_1$ window around i with respect to the distance measure on the manifold

Compute by a gradient descent algorithm the Karcher mean patch, $\hat{\boldsymbol{\mu}}_i = (\hat{\boldsymbol{\mu}}_{i,j})_{j=1}^{s_1^2}$,

$$\hat{\boldsymbol{\mu}}_i \in \arg \min_{\mathbf{y} \in \mathcal{M}} \left\{ \frac{1}{K_1} \sum_{j \in \mathcal{S}_1(i)} \text{dist}_M(\mathbf{y}, \mathbf{y}_j)^2 \right\}$$

Homogeneous area test: Compute by a gradient descent algorithm the Karcher mean value $\hat{\mathbf{m}}_i \in \arg \min_{\mathbf{y} \in M} \left\{ \frac{1}{K_1 s_1^2} \sum_{j \in \mathcal{S}_1(i)} \sum_{k=1}^{s_1^2} \text{dist}_M(\mathbf{y}, \mathbf{y}_{j,k})^2 \right\}$ and the empirical variance of the patches

$$\hat{\sigma}_i^2 = \frac{1}{dK_1 s_1^2} \sum_{j \in \mathcal{S}_1(i)} \sum_{k=1}^{s_1^2} \text{dist}_M(\hat{\mathbf{m}}_i, \mathbf{y}_{j,k})^2$$

if $\hat{\sigma}_i^2 \leq \gamma \sigma^2$ **then**

Compute the restored patches as $\hat{\mathbf{y}}_j = \mathbf{1}_{s_2^2} \otimes \hat{\mathbf{m}}_i$, $j \in \mathcal{S}_1(i)$

else

Compute the empirical covariance matrix

$$\hat{\Sigma}_i = \frac{1}{K_1} \sum_{j \in \mathcal{S}_1(i)} \log_{\hat{\boldsymbol{\mu}}_i}(\mathbf{y}_j) \log_{\hat{\boldsymbol{\mu}}_i}(\mathbf{y}_j)^\top$$

Compute the restored patch $\hat{\mathbf{y}}_j = \exp_{\hat{\boldsymbol{\mu}}_i}((\hat{\Sigma}_i - \sigma^2 I_{s_1^2}) \hat{\Sigma}_i^{-1} \log_{\hat{\boldsymbol{\mu}}_i}(\mathbf{y}_j))$, $j \in \mathcal{S}_1(i)$

Aggregation: Obtain the first estimate $\hat{\mathbf{y}}$ at each pixel by computing the Karcher mean over all restored patches containing the pixel

Algorithm 2 Nonlocal MMSE Denoising Algorithm, Step 2

Step 2:

 Set $\mathcal{M} = M^{s_2^2}$
for all patches \mathbf{y}_i of the noisy image \mathbf{y} not considered before **do**

 Determine the set $\mathcal{S}_2(i)$ of centers of K_2 patches similar to the denoised image $\hat{\mathbf{y}}_i$ in the first step in a $w_2 \times w_2$ window around i

 Compute the Karcher mean patch, $\hat{\mu}_i = (\hat{\mu}_{i,j})_{j=1}^{s_1^2}$,

$$\tilde{\mu}_i \in \arg \min_{\mathbf{y} \in \mathcal{M}} \left\{ \frac{1}{K_2} \sum_{j \in \mathcal{S}_2(i)} \text{dist}_{\mathcal{M}}(\mathbf{y}, \mathbf{y}_j)^2 \right\}$$

Homogeneous area test: Compute the Karcher mean value $\tilde{\mathbf{m}}_i \in \arg \min_{\mathbf{y} \in \mathcal{M}} \left\{ \frac{1}{K_2 s_2^2} \sum_{j \in \mathcal{S}_2(i)} \sum_{k=1}^{s_2^2} \text{dist}_M(\mathbf{y}, \mathbf{y}_{j,k})^2 \right\}$ and the empirical variance of the patches

$$\tilde{\sigma}_i^2 = \frac{1}{dK_2 s_2^2} \sum_{j \in \mathcal{S}_2(i)} \sum_{k=1}^{s_2^2} \text{dist}_M(\tilde{\mathbf{m}}_i, \mathbf{y}_{j,k})^2$$

if $\tilde{\sigma}_i^2 \leq \gamma \sigma^2$ **then**

 Compute the restored patches $\tilde{\mathbf{y}}_j = \mathbf{1}_{s_2^2} \otimes \tilde{\mathbf{m}}_i$, $j \in \mathcal{S}_2(i)$
else

Compute the empirical covariance matrix

$$\tilde{\Sigma}_i = \frac{1}{K_2} \sum_{j \in \mathcal{S}_1(i)} \log_{\tilde{\mu}_i}(\hat{\mathbf{y}}_j) \log_{\tilde{\mu}_i}(\hat{\mathbf{y}}_j)^T + \sigma^2 I_{s_2^2}$$

 Compute the restored patch $\tilde{\mathbf{y}}_j = \exp_{\tilde{\mu}_i}((\tilde{\Sigma}_i - \sigma^2 I_{s_2^2}) \tilde{\Sigma}_i^{-1} \log_{\tilde{\mu}_i}(\mathbf{y}_j))$, $j \in \mathcal{S}_2(i)$

Aggregation: Obtain the final estimate $\tilde{\mathbf{y}}$ at each pixel by computing the Karcher mean over all restored patches containing the pixel

5. Numerical Results

In this section we provide numerical examples to illustrate the good performance of the NL-MMSE Algorithm 2. As manifolds we consider the circle \mathbb{S}^1 , the sphere \mathbb{S}^2 and the positive definite matrices $\text{SPD}(r)$ for $r = 2, 3$. While Algorithm 2 is implemented in MATLAB, the basic manifold functions, like logarithmic and exponential maps, as well as the distance function are implemented as C++ functions in „Manifold-valued Image Restoration Toolbox“ (MVIRT)¹ and imported into MATLAB using mex-interfaces with the GCC 4.8.4 compiler. The experiments are carried out on a Dell Precision T1500 running Ubuntu 14.04 LTS, Core i7, 2.93 GHz, and 8 GB RAM, using MATLAB 2014b.

To compare different methods we used as performance measure the mean squared error

$$\epsilon = \frac{1}{N} \sum_{i \in \mathcal{G}} \text{dist}_M(\hat{\mathbf{x}}_i, \mathbf{x}_i)^2,$$

where x denotes the original image and \hat{x} is the restored one. The parameters of all involved algorithms were optimized with respect to this error measure on the grids detailed below. We compared the following denoising methods:

- (i) **NL-MMSE**: we implemented Algorithm 2 with parameters from the following grid search (in MATLAB notation): patch size $s \in \{3 : 2 : 11\}$, window size $w \in \{9 : 2 : 127\}$, number of neighbors $K \in \{1 : 1 : 1200\}$, and $\gamma \in \{0.1 : 0.1 : 2\}$. We would like to mention that we started on coarser grids and refined them during the parameter search. We briefly comment on general guidelines for the parameter in the following subsection. The final parameters for our experiments are listed in Table 2. Note that in the first three experiments we optimized only one set of parameters, i.e., they are the same in both steps, while the parameters for both steps are optimized for the last three examples.
- (ii) **NL-means**: we implemented a generalization of the NL-means algorithm [14, 63] for manifold-valued images. Since this algorithm is not available in the general form required for our noisy images, we describe it in the next subsection. Concerning the grid search we used the same grids as in (i) for s, w, K . Further, δ is optimized on $\{0.5 : 0.5 : 50\}$, and τ on $\{0.1 : 0.1 : 1\}$.
- (iii) **TV approach**: we applied the manifold version of the variational denoising approach with $\text{dist}_{\mathcal{M}}^2$ as data fidelity term and anisotropic discrete total variation (TV) term as proposed in [76]. Furthermore, for cyclic data we also added a second regularization term to (iii), called TV_2 , which is a manifold version of second order differences. This method was proposed for the circle in [10] and for more general symmetric spaces in [7] and we used the corresponding programs. Using the notation from [7], we did a grid search for the regularization parameter α of the TV term in $\{0.01 : 0.01 : 1\}$ and for the regularization parameter β of the TV_2 term in $\{0.1 : 0.1 : 5\}$. The main drawback of the variational methods are their extensive running time compared to (i) and (ii).

¹<http://www.mathematik.uni-kl.de/imagepro/members/bergmann/mvirt/>

Figure	s_1	s_2	w_1	w_2	K_1	K_2	γ
Figure 4 (d)	7	7	81	81	70	70	1
Figure 4 (h)	5	5	37	37	110	110	1
Figure 5	5	5	59	59	415	415	.8
Figure 6	9	9	115	115	1038	1038	1
Figure 7	9	7	119	123	186	86	1.1
Figure 8	3	5	127	127	65	54	0.8

Table 2. Parameters for the NL-MMSE Algorithm 2 in the examples.

5.1. Parameter Selection

Our algorithm requires several input parameters. Besides the variance σ^2 of the noise (which is assumed to be known or otherwise may be estimated in constant areas), these are the size of the patches and of the search zone as well as the number of similar patches that are kept and a parameter for the homogeneous area criterion. Even if it is not possible to state general parameter constellations that are valid for the different manifolds there are some general principles how to choose good parameters. Based on these principles we may obtain a first set of parameters, which may be fine-tuned by varying one of them while keeping the rest fixed.

- (i) patch size s : In general, the considered patches are rather small ($s \in \{3, 5, 7\}$), their exact value depends on the amount of noise, measured in terms of the variance σ^2 of the noise. The higher the noise, the larger the patches, as they contain less information when the noise level is high.
- (ii) window size w : The size of the search zone depends on the one hand on the patch size and on the other hand on the number of similar patches, which depends itself on the dimension of the manifold. The larger those values are, the larger the search zone should be.
- (iii) number of similar patches K : The number of similar patches has to be large enough to guarantee that the estimated covariance matrix is invertible with high probability, which depends on the patch size and on the dimension d of the manifold. On the other hand, it should also not be too large as in this case also non-similar patches are chosen. As a rule of thumb we observed that $K = 3s^2d$ yields good results in practice.
- (iv) homogeneous area parameter γ : This value should be close to 1 and it should be the larger, the more constant areas an image contains.

5.2. Nonlocal Means on Manifolds

In this section we briefly discuss how to generalize the NL-means approach introduced in [14] to manifolds. The fundamental difference to the NL-MMSE lies, besides some details, in the incorporation of second order information.

Let $y: \mathcal{G} \rightarrow M$ be a noisy manifold-valued image. Consider a $s \times s$ patch $y_i \in M^{s^2}$ centered at $i = (i_1, i_2) \in \mathcal{G}$. For each $i \in \mathcal{G}$ we denote by $\mathcal{S}(i)$ the set of K similar patches

to y_i , selected in a $w \times w$ search window around y_i . Similar patches are found with respect to a weighted distance on the product manifold, i.e.,

$$\widetilde{\text{dist}}_{M^{s^2}}(y_i, y_j)^2 := \sum_{k_1 = -\lfloor \frac{s-1}{2} \rfloor}^{\lfloor \frac{s-1}{2} \rfloor} \sum_{k_2 = -\lfloor \frac{s-1}{2} \rfloor}^{\lfloor \frac{s-1}{2} \rfloor} e^{-\frac{1}{2\delta^2}(k_1^2+k_2^2)} \text{dist}_M(y_{i_1+k_1, i_2+k_2}, y_{j_1+k_1, j_2+k_2})^2, \quad (24)$$

where $\delta > 0$, $y_i \in M^{s^2}$ denotes the whole patch and $y_{i_1, i_2} \in M$ denotes a pixel value. The aggregation step is done by averaging the patch centers, weighted by the distance of the patches, i.e., let

$$\omega_{i,j} = \begin{cases} e^{-\frac{1}{2\tau^2}\widetilde{\text{dist}}_{M^{s^2}}(y_i, y_j)^2} & i \neq j, \\ \max_{j \in \mathcal{S}(i), j \neq i} \{\omega_{i,j}\} & i = j, \end{cases} \quad \text{and} \quad W_i = \sum_{j \in \mathcal{S}(i)} \omega_{i,j}. \quad (25)$$

Then the restored pixel value is given by

$$\hat{y}_i = \arg \min_{y \in M} \left\{ \frac{1}{W_i} \sum_{j \in \mathcal{S}(i)} \omega_{i,j} \text{dist}_M(y, y_j)^2 \right\}. \quad (26)$$

For the weights in (25) we use the maximal weight approach for the center patch, which was proposed in [63] as the best choice without introducing an extra parameter.

Let us briefly comment on two related approaches. A NL-means denoising algorithm for DT-MRI images was given in [77]. The authors use the affine invariant distance on $\text{SPD}(r)$ as similarity measure in (24) and the log-Euclidean mean for computing the mean (26), while we perform both steps with the same affine invariant distance measure. The authors of [55] introduce a semi-local method for denoising manifold-valued data motivated by the corresponding variational method for real valued data. Their method performs an iterative averaging over circular shaped neighborhoods with weights depending on the pixel similarity and distances between the pixels on the image grid. In contrast to [55] we consider patches around the pixels for computing their similarity.

5.3. Noise on Color Channels

Manifold-valued images naturally appear in various color image models different from the RGB model. In the following, we consider the hue-saturation-value (HSV) and the chromaticity-brightness (CB) color model. We added Gaussian noise to the hue and the chromaticity channels. We are aware of the fact, that natural color images are in general not corrupted by Gaussian noise in only one color channel. However, we provide these academical examples as a proof of concept. How such single channel noise affects the whole image can be seen in Figure 3.

Cyclic data appears in the hue component of the HSV color model. The hue component of the *sponge* is considered in the first row of Figure 4. The second column 4 (b) shows the noisy hue corrupted by wrapped Gaussian noise of standard deviation $\sigma = 0.6$. Applying the TV denoising method with optimized parameters $\alpha = 0.45$, $\lambda = \frac{\pi}{2}$, resp., NL-MMSE, leads to the results in Figure 4 (c), resp. Figure 4 (d). Despite rather flat areas in the image, the NL-MMSE approach outperforms the variational TV method.

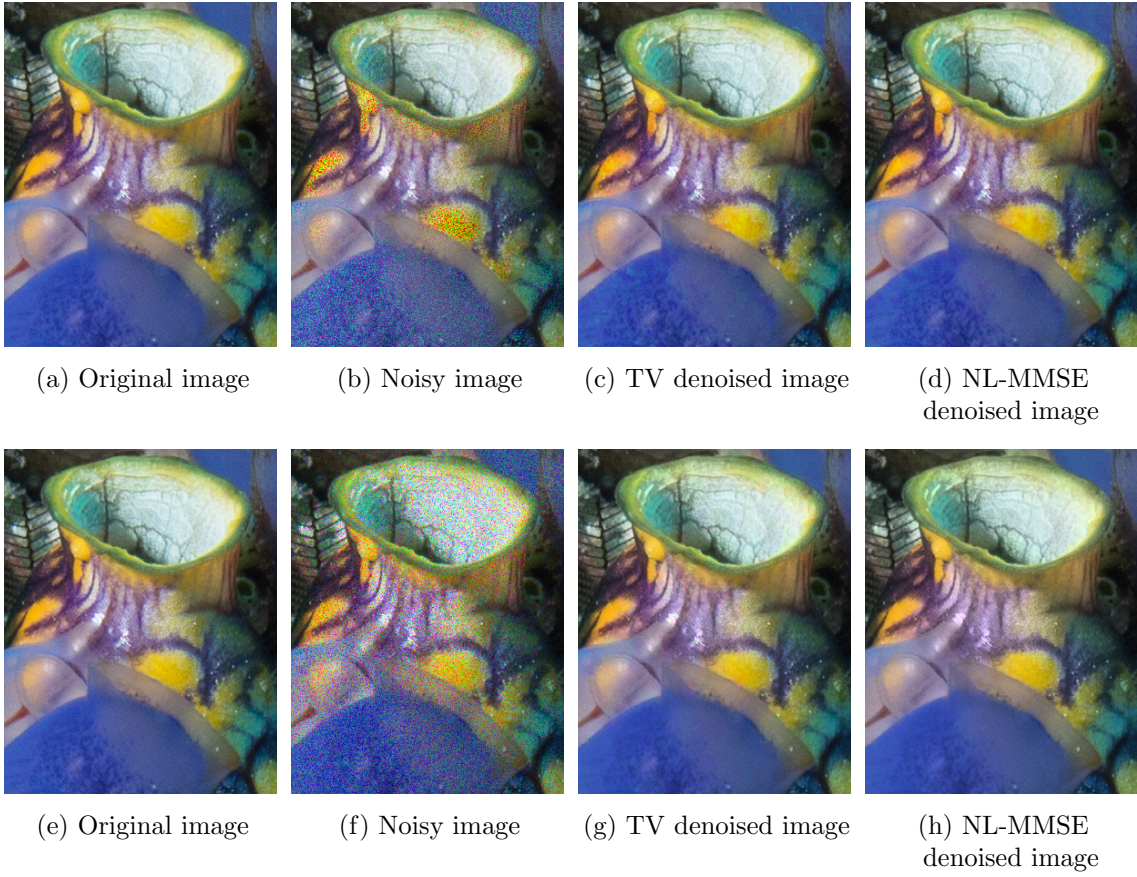


Figure 3. Original (first column), noisy (second column), TV denoised (third column) and NL-MMSE denoised (fourth column) sponge image in the HSV (top row) and the CB (bottom row) color space.

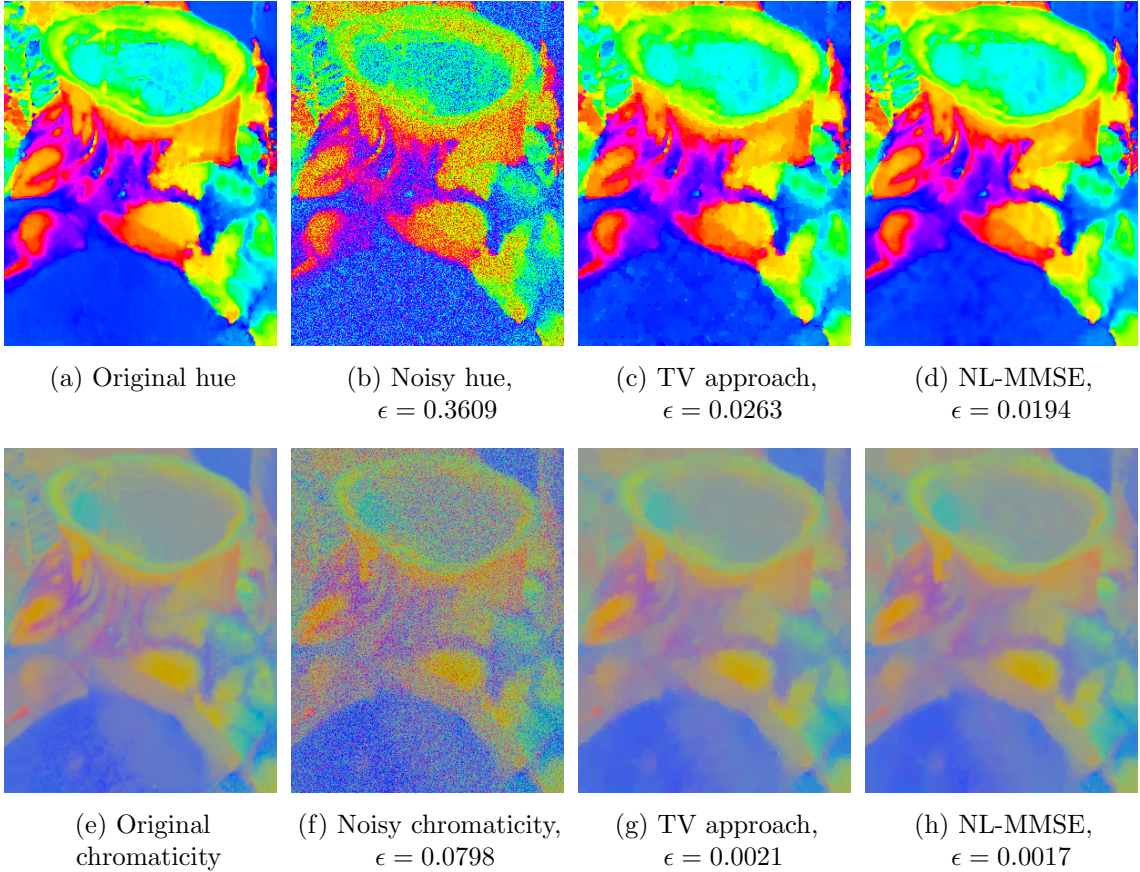


Figure 4. Denoising the hue and chromaticity of the color image *sponge*.

Spherical data occurs in the chromaticity component of the CB color space. At this point, the chromaticity is defined as the direction of the RGB color vector and the brightness is given by its length. We deal with the chromaticity of the *sponge* image in the second row of Figure 4. We corrupted it by Gaussian noise of standard deviation $\sigma = 0.2$, which yields the image shown in Figure 4 (f). Figure 4 (g) gives the result of the TV method with $\alpha = 0.21$, $\lambda = \frac{\pi}{2}$. Denoising with the NL-MMSE results in Figure 4 (h) which is again better than the previous one.

5.4. Matrix-Valued Data

In this subsection, we provide two examples for images having values in $\text{SPD}(r)$ for $r = 2, 3$. A matrix $\mathbf{x} \in \text{SPD}(r)$, $r = 2, 3$, is depicted as an ellipse ($r = 2$) or an ellipsoid ($r = 3$) whose principal axis are determined by the spectral decomposition of \mathbf{x} .

First we examine the effect of the acceleration used in the NL-MMSE approach. To this aim we consider the 64×64 image with $\text{SPD}(3)$ values depicted in Figure 5 (a). The image is corrupted by Gaussian noise of standard deviation $\sigma = 0.125$, see Figure 5 (b). Using NL-MMSE yields Figure 5 (c). Taking all pixels as center of a reference patch, i.e., skipping the acceleration, gives the result in Figure 5 (d). Visually, there is nearly no difference

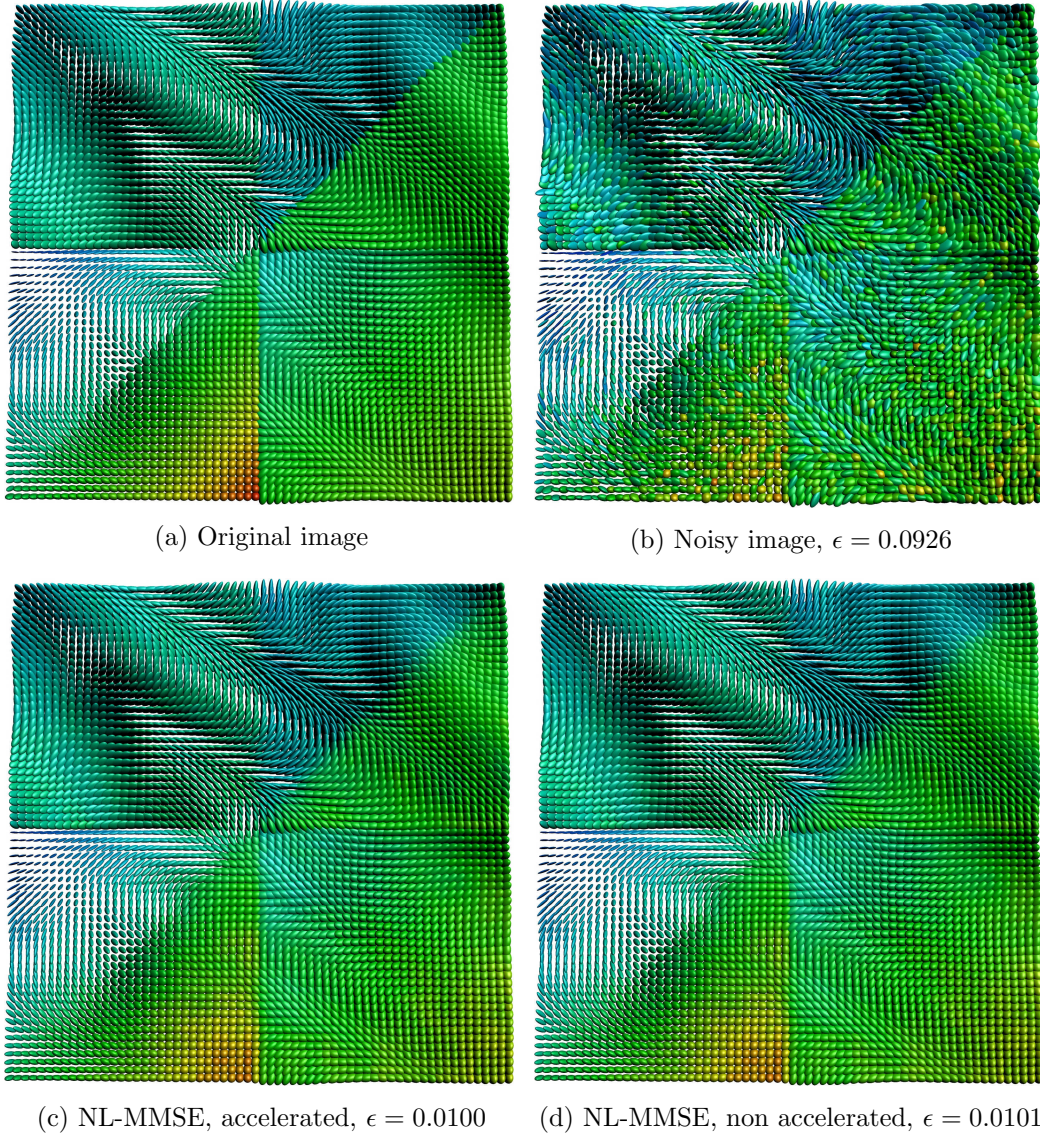


Figure 5. Denoising an image with values in $\text{SPD}(3)$ using NL-MMSE with and without acceleration.

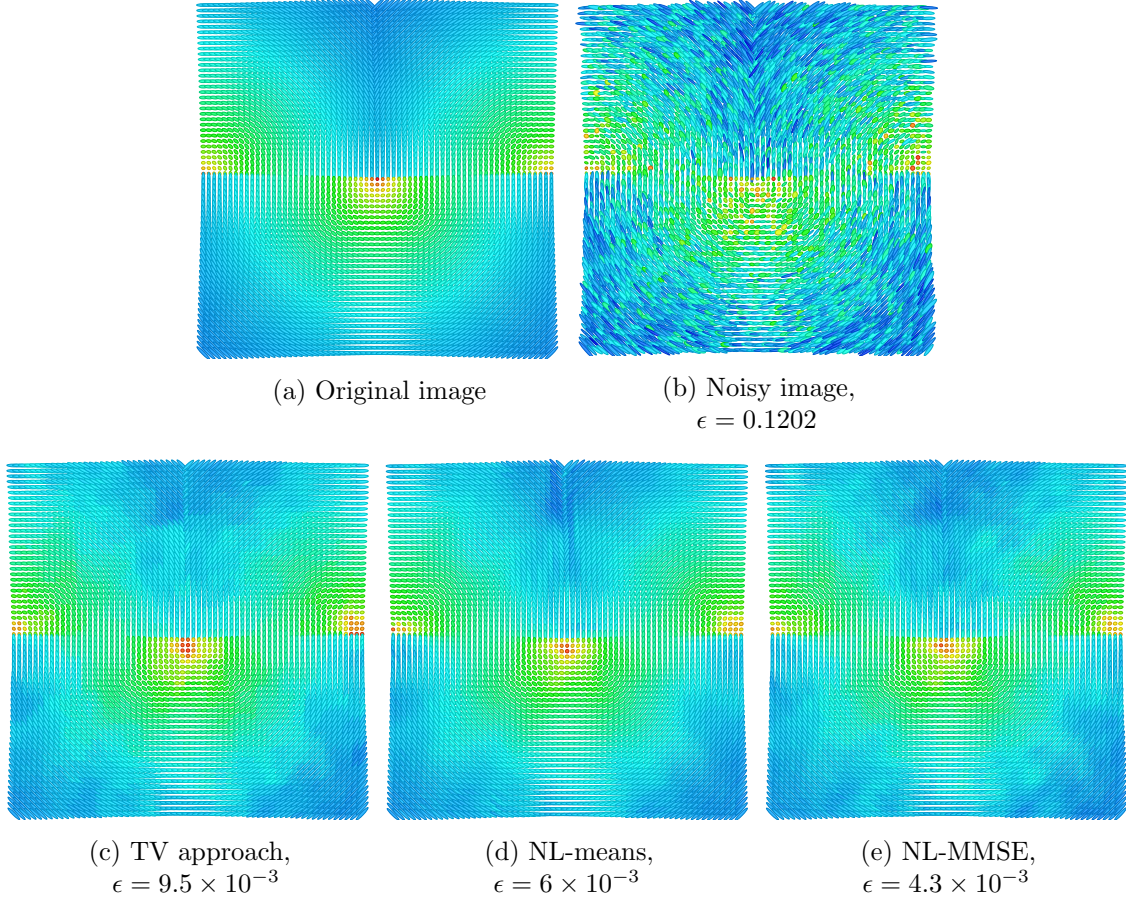


Figure 6. Comparison of denoising methods for an image with values in $\text{SPD}(2)$.

between the two results, and also the errors are roughly the same. However, having a look at the running time there is a large difference between the two approaches. The accelerated algorithm needs 245 seconds and is about one hundred times faster as the non-accelerated version, which needs 40691 seconds. This justifies the acceleration step.

Next consider the artificial image of size 65×65 consisting of $\text{SPD}(2)$ matrices in Figure 6(a) and its corrupted version with Gaussian noise of standard deviation $\sigma = 0.15$ in Figure 6(b). In the denoising result with the TV method with parameters $\alpha = 0.25$, $\gamma = 1$ in Figure 6(c), the typical stair casing effect is visible. Figure 6(d) depicts the result of NL-means using the optimized parameters $s = 33$, $w = 9$, $\delta = 2$, $K = 81$, $\tau = 0.2$ which looks better than the previous one. However, the NL-MMSE with the same parameters for both steps yields a denoised image with error $\epsilon = 0.0049$, and changing the parameters of the second step to $s_2 = 7$, $K_2 = 193$, $w_2 = 41$ we finally obtain an error of $\epsilon = 0.0042$, compare Figure 6(e). This error is a lower than those of the TV and NL-means methods. Moreover, this example shows that different parameters in both steps allow a further improvement of the algorithm. In the following examples we optimize the parameters of both steps separately.

5.5. Cyclic Data

Next we compare the proposed NL-MMSE for the artificial image in Figure 7 (a) and its noisy version corrupt with wrapped Gaussian noise of standard deviation $\sigma = 0.3$ in Figure 7 (b). These images as well as their denoised versions via the TV approach and the TV-TV₂ method were taken from [10]. The original image can be found in the toolbox MVIRT. The TV approach leads to the result in Figure 7 (c). While the jumps between flat areas are preserved, the method suffers from stair casing. The combined first and second order approach in Figure 7 (d) improves the results, but the edges between flat areas are smoothed. Not surprisingly, the result obtained with the NL-means approach in Figure 7 (e) with parameters $s = 11, w = 23, \delta = 46, K = 33, \tau = 0.2$ has the worst error, even if the reconstructions of the paraboloid in the bottom right and at the edges are pretty good. Here an extra fitting for constant regions as incorporated in the fine tuning of NL-MMSE, would be necessary. The best result, shown in Figure 7 (f), is achieved with the NL-MMSE, see Figure 7 (f). On the one hand, sharp edges are preserved, while on the other hand also constant and linear parts are well reconstructed.

5.6. Spherical Data

Finally we consider the artificial image with values distributed over the whole sphere as shown in Figure 8 (a). The image consists of vortex like structures of different sizes and directions and a smoothly varying background. It is affected by Gaussian noise with standard deviation $\sigma = 0.3$, see Figure 8 (b). We compare our method with the TV approach (parameters: $\alpha = 0.24, \gamma = \frac{\pi}{2}$) in Figure 8 (c), TV-TV₂ (parameters: $\alpha = 0.18, \beta = 2.6, \gamma = \frac{\pi}{2}$) in Figure 8 (d), and NL-means (parameters: $\epsilon, s = 23, w = 127, \delta = 1.5, K = 104, \tau = 0.2$) in Figure 8 (e). Note that the running time of the NL-mean is the same as the NL-MMSE in this example, i.e., 20 seconds, while the TV-TV₂ method needs around minutes. The first order TV suffers from stair casing, which is removed with the second order term, but the error is still the largest among all tested methods. Next we have a look at the oracle image after Step 1 of NL-MMSE in Figure 8 (f). We see that this image has already a slightly smaller error than both TV and the NL-means approaches. However, it still contains some noise in the background, which is removed in the second step and leads to an improvement in the error, see Figure 8 (g).

Figure 8 (h) shows the reconstruction with Algorithm 2 without the second order-update step, i.e., we perform only Step 1, where we replace $\hat{\mathbf{y}}_j = \exp_{\hat{\boldsymbol{\mu}}_i}(\hat{\boldsymbol{\Sigma}}_i(\hat{\boldsymbol{\Sigma}}_i + \sigma^2 I_{s_1^2})^{-1} \log_{\hat{\boldsymbol{\mu}}_i}(y_j))$ with $\hat{\mathbf{y}}_j = \hat{\boldsymbol{\mu}}_i$. The parameters are $s = 5, K = 6$ and w, γ from before. In comparison to the oracle image there are small visible differences, but the error is worse. A disadvantage of this method is its running time. While the oracle image computation needs less than 10 seconds, about 30 seconds are required to get the result in Figure 8 (h). The time difference originates from the larger patch size which is needed to get a comparable result.

This experiment further shows that Algorithm 2 is also able to handle data having values on the whole sphere which is a manifold with positive curvature. Here, we implicitly assume that the computed Karcher means are unique, which is a reasonable assumption, since similar patches should be pointwise contained in regular balls. Note that this does not prevent the patches to cover the whole sphere.

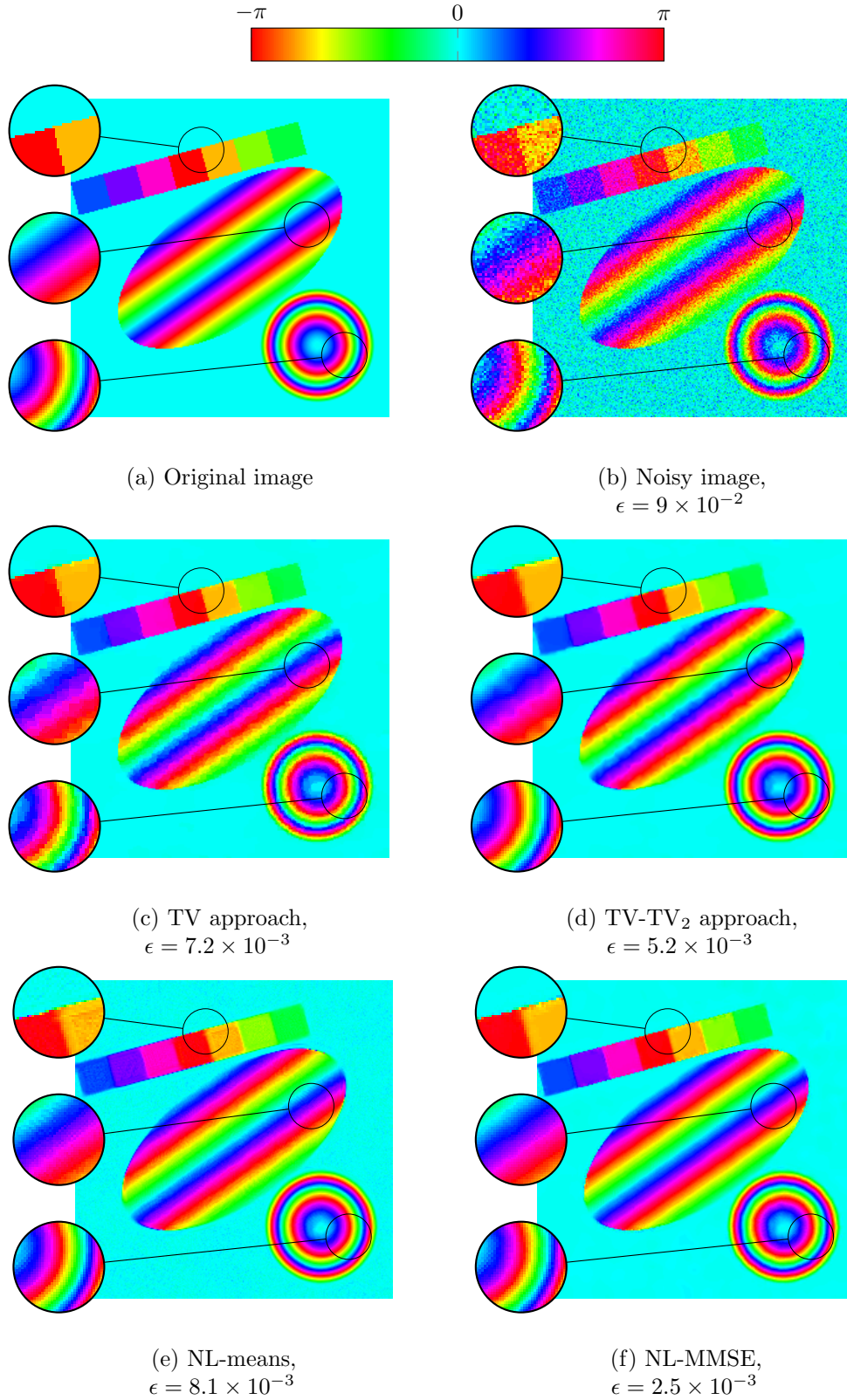


Figure 7. Comparison of denoising methods for an image with values in \mathbb{S}^1 .

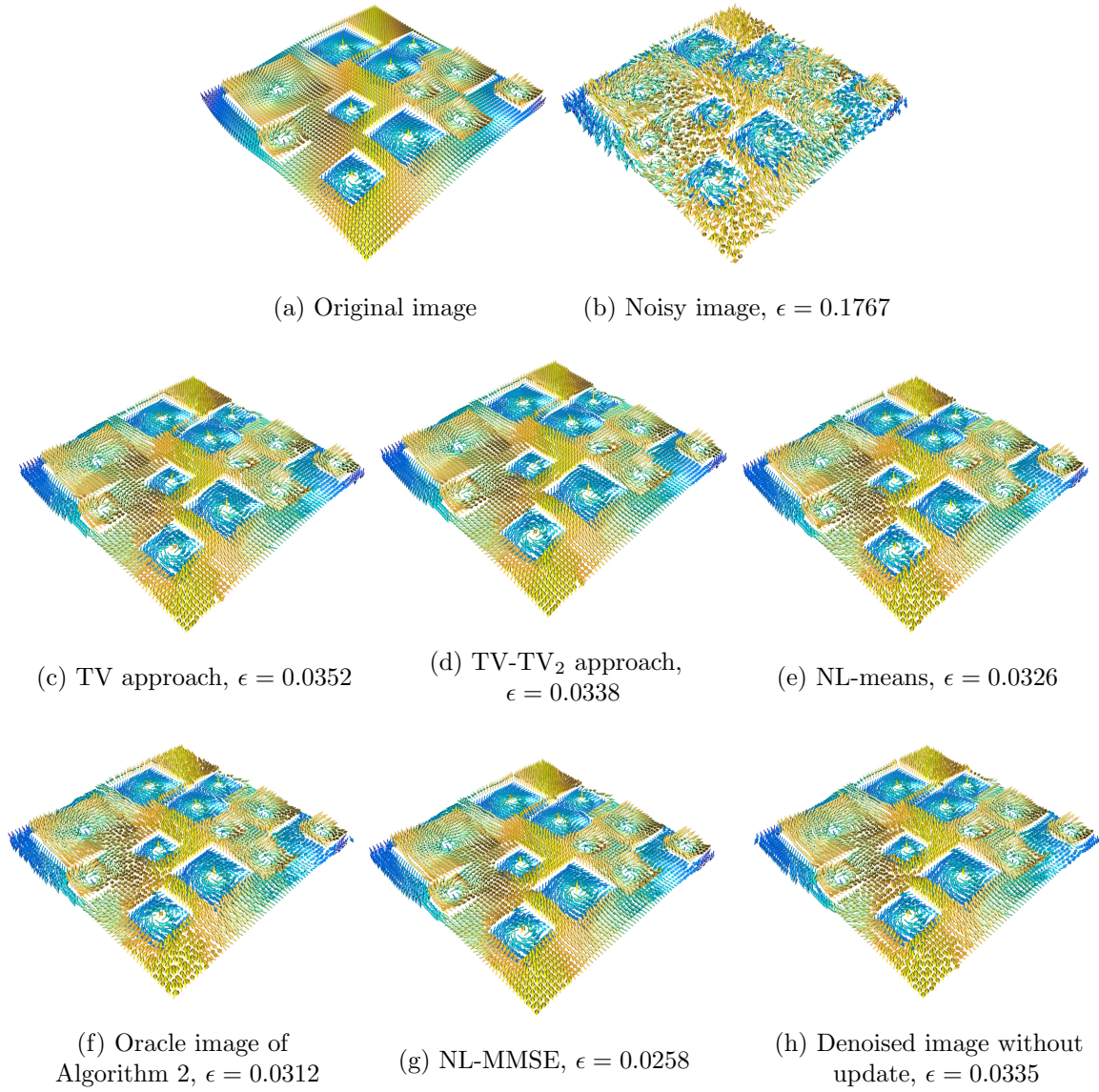


Figure 8. Comparison of denoising methods of an S^2 -valued image.

6. Conclusion and Future Work

We proposed a counterpart of the nonlocal Bayes' denoising approach of Lebrun et al. [40, 41] for manifold-valued images. The basic idea consists in translating the MMSE for similar image patches (8) to the manifold-valued setting (23). To this aim, we used an intrinsic definition of a normal distribution and in particular of white noise on Riemannian manifolds. We demonstrated by various numerical experiments that our method performs very well when dealing with moderate noise variances.

Up to now all our examples were artificial ones. In future work we want to apply our method to real-world data. In particular we intend to examine whether our noise model covers specific applications. The close relation between different models of Gaussian noise for small σ should be specified for the manifolds of interest. Moreover, it is well known that in various applications the variance σ^2 is either not known or not constant for the whole image. Therefore the noise estimation and the incorporation of spatially varying noise is an interesting research topic.

Another issue is related to Remark 2.4. Even in the Euclidean setting the topic of negative eigenvalues in the estimation of Σ_X requires further discussion. Other directions of future work include other image restoration tasks as for instance inpainting. This needs additional information, e.g., based on hyperpriors as in [3] or a fixed number of Gaussian models (covariance matrices), see e.g. [80].

A. Proof of Proposition 4.1

Proof. For one-dimensional manifolds we have $x = x^1$ and $|G(x)| = |\tilde{G}(\mathbf{x})| = 1$. In the following we set $e_\mu := e_{\mu,1}$.

(i) With Appendix B we obtain $\text{dist}_{\text{SPD}(1)}(\boldsymbol{\mu}, \mathbf{x}) = \left| \ln\left(\frac{\mu}{x}\right) \right|$ so that with (17) we obtain the pdf stated in (i). By (15) we have

$$\frac{1}{\sqrt{2\pi\sigma^2}} \int_{\mathbb{R}} e^{-\frac{1}{2\sigma^2}x^2} dx = \frac{1}{\sqrt{2\pi\sigma^2}} \int_{\mathbb{R}_{>0}} e^{-\frac{1}{2\sigma^2}(\ln(x)-\ln(\mu))^2} d_{\mathbb{R}_{>0}}(\mathbf{x})$$

which implies by the transformation theorem that $d_{\mathbb{R}_{>0}}(\mathbf{x}) = \frac{1}{x} d\mathbf{x}$.

(ii) In the given parameterization it holds that $e_\mu = (-\sin(t_\mu), \cos(t_\mu))^T$, $t_\mu \in [-\pi, \pi)$ and with Appendix B further

$$\exp_\mu(h(x)) = \exp_\mu(xe_\mu) = \boldsymbol{\mu} \cos(|x|) + \frac{x}{|x|} \sin(|x|)e_\mu = \begin{pmatrix} \cos(x + t_\mu) \\ \sin(x + t_\mu) \end{pmatrix}.$$

It holds $\mathcal{D}_\mu = (-\pi, \pi)$ and we can choose $\varphi_j: ((2j-1)\pi, (2j+1)\pi) \rightarrow (-\pi, \pi)$ as $\varphi_j(x) := x - 2j\pi$, $j \in \mathbb{Z}$ in (18). Plugging this into (17) results in

$$\begin{aligned} p_{\mathbf{X}}(\mathbf{x}(t)) &= \frac{1}{\sqrt{2\pi\sigma^2}} \sum_{j \in \mathbb{Z}} e^{-\frac{1}{2\sigma^2}(h^{-1}(\log_\mu(\mathbf{x}(t))) + 2j\pi)^2} = \frac{1}{\sqrt{2\pi\sigma^2}} \sum_{j \in \mathbb{Z}} e^{-\frac{1}{2\sigma^2}(d_{\mathbb{S}^1}(\boldsymbol{\mu}, \mathbf{x}(t)) + 2j\pi)^2} \\ &= \frac{1}{\sqrt{2\pi\sigma^2}} \sum_{j \in \mathbb{Z}} e^{-\frac{1}{2\sigma^2}(t - t_\mu + 2j\pi)^2}. \end{aligned}$$

(iii) First note that Δ_1 is not complete, but for any $\boldsymbol{\mu}$ the function $\exp_{\boldsymbol{\mu}}$ is defined a.e. on $T_{\boldsymbol{\mu}}\Delta_1$. More precisely, using Appendix B we obtain $e_{\boldsymbol{\mu}} = \frac{1}{2} \sin(t_{\boldsymbol{\mu}})(1, -1)^{\text{T}}$ and

$$\exp_{\boldsymbol{\mu}}(h(x)) = \frac{1}{2} + \frac{1}{2} \begin{pmatrix} \cos(t_{\boldsymbol{\mu}}) \\ -\cos(t_{\boldsymbol{\mu}}) \end{pmatrix} \cos(x) + \frac{1}{2} \begin{pmatrix} \sin(t_{\boldsymbol{\mu}}) \\ -\sin(t_{\boldsymbol{\mu}}) \end{pmatrix} \sin(x) = \frac{1}{2} + \frac{1}{2} \begin{pmatrix} \cos(x - t_{\boldsymbol{\mu}}) \\ -\cos(x - t_{\boldsymbol{\mu}}) \end{pmatrix},$$

which is only in Δ_1 if $x \notin \{t_{\boldsymbol{\mu}} + j\pi : j \in \mathbb{Z}\}$. Here have $\mathcal{D}_{\boldsymbol{\mu}} = (t_{\boldsymbol{\mu}} - \pi, t_{\boldsymbol{\mu}})$ and setting

$$\begin{aligned} \varphi_{2j}(x) &:= x - 2j\pi \quad \text{for } x \in (t_{\boldsymbol{\mu}} + (2j - 1)\pi, t_{\boldsymbol{\mu}} + 2j\pi), \\ \varphi_{2j+1}(x) &:= 2t_{\boldsymbol{\mu}} - (x - 2j\pi) \quad \text{for } x \in (t_{\boldsymbol{\mu}} + 2j\pi, t_{\boldsymbol{\mu}} + (2j + 1)\pi) \end{aligned}$$

we obtain by (18) that

$$\tilde{p}_X(x) = \frac{1}{\sqrt{2\pi\sigma^2}} \sum_{j \in \mathbb{Z}} \left(e^{-\frac{1}{2\sigma^2}(x+2j\pi)^2} + e^{-\frac{1}{2\sigma^2}(2t_{\boldsymbol{\mu}}-x+2j\pi)^2} \right).$$

With (17) we obtain the assertion. □

B. Example Manifolds

Sphere \mathbb{S}^d Let $\mathbb{S}^d = \{\boldsymbol{x} \in \mathbb{R}^{d+1} : \|\boldsymbol{x}\|_2 = 1\}$. The geodesic distance is given by

$$\text{dist}_{\mathbb{S}^d}(\boldsymbol{x}, \boldsymbol{y}) = \arccos(\langle \boldsymbol{x}, \boldsymbol{y} \rangle),$$

where $\langle \cdot, \cdot \rangle$ is the standard scalar product in \mathbb{R}^{d+1} . The tangential space at $\boldsymbol{x} \in \mathbb{S}^d$ is given by $T_{\boldsymbol{x}}\mathbb{S}^d = \{v \in \mathbb{R}^{d+1} | \langle \boldsymbol{x}, v \rangle = 0\}$. The Riemannian metric is the metric from the embedding space, i.e., the Euclidean inner product. The exponential and logarithmic map read as

$$\begin{aligned} \exp_{\boldsymbol{x}}(v) &= \boldsymbol{x} \cos(\|v\|) + \frac{v}{\|v\|} \sin(\|v\|), \\ \log_{\boldsymbol{x}}(\boldsymbol{y}) &= \text{dist}_{\mathbb{S}^d}(\boldsymbol{x}, \boldsymbol{y}) \frac{\boldsymbol{y} - \langle \boldsymbol{x}, \boldsymbol{y} \rangle \boldsymbol{x}}{\|\boldsymbol{y} - \langle \boldsymbol{x}, \boldsymbol{y} \rangle \boldsymbol{x}\|}, \quad \boldsymbol{x} \neq -\boldsymbol{y}. \end{aligned}$$

Positive Definite Matrices $\text{SPD}(r)$ The dimension of $\text{SPD}(r)$ is $d = \frac{r(r+1)}{2}$. We denote by Exp and Log the matrix exponential and logarithm defined by $\text{Exp}(x) := \sum_{k=0}^{\infty} \frac{1}{k!} x^k$ and $\text{Log}(x) := -\sum_{k=1}^{\infty} \frac{1}{k} (I - x)^k$, $\rho(I - x) < 1$, where ρ denotes the spectral radius. Then the affine invariant geodesic distance is given by

$$\text{dist}_{\text{SPD}(r)}(\boldsymbol{x}, \boldsymbol{y}) = \left\| \text{Log}(\boldsymbol{x}^{-\frac{1}{2}} \boldsymbol{y} \boldsymbol{x}^{-\frac{1}{2}}) \right\|_{\text{F}},$$

where $\|\cdot\|_{\text{F}}$ denotes the Frobenius norm of matrices. The tangential space at $\boldsymbol{x} \in \mathcal{M}$ is $T_{\boldsymbol{x}}\mathcal{M} = \{\boldsymbol{x}\} \times \text{Sym}(r)$, where Sym denotes the space of symmetric $r \times r$ matrices. The Riemannian metric reads $\langle v_1, v_2 \rangle_{\boldsymbol{x}} = \text{tr}(v_1 \boldsymbol{x}^{-1} v_2 \boldsymbol{x}^{-1})$. As orthogonal basis in $T_{\boldsymbol{x}}\mathcal{M}$ we use $e_{\boldsymbol{x},ij} := \boldsymbol{x}^{\frac{1}{2}} e_{ij} \boldsymbol{x}^{\frac{1}{2}}$, $i, j \in \{1, \dots, r\}$, $j \leq i$, where

$$e_{ij} = \begin{cases} e_i e_i^{\text{T}} & \text{if } i = j, \\ \frac{1}{\sqrt{2}} (e_i e_j^{\text{T}} + e_j e_i^{\text{T}}) & \text{otherwise} \end{cases}$$

and $e_i \in \mathbb{R}^r$ are the r -dimensional unit vectors. Finally, the exponential and the logarithmic map read

$$\begin{aligned}\exp_{\mathbf{x}}(v) &= \mathbf{x}^{\frac{1}{2}} \text{Exp}(\mathbf{x}^{-\frac{1}{2}} v \mathbf{x}^{-\frac{1}{2}}) \mathbf{x}^{\frac{1}{2}}, \\ \log_{\mathbf{x}}(\mathbf{y}) &= \mathbf{x}^{\frac{1}{2}} \text{Log}(\mathbf{x}^{-\frac{1}{2}} \mathbf{y} \mathbf{x}^{-\frac{1}{2}}) \mathbf{x}^{\frac{1}{2}}.\end{aligned}$$

For more information on the affine invariant metric and its relation to the log-Euclidean metric we refer, e.g., to [5, 54],

Probability Simplex Δ_d In the open probability simplex $\Delta_d := \{\mathbf{x} \in \mathbb{R}_{>0}^{d+1} : \sum_{i=1}^{d+1} x_i = 1\}$ equipped with the Fisher-Rao metric arising from the categorical distribution $\langle u, v \rangle_{\mathbf{x}} = \langle \frac{u}{\sqrt{\mathbf{x}}}, \frac{v}{\sqrt{\mathbf{x}}} \rangle$ the geodesic distance is given by

$$\text{dist}_{\Delta_d}(\mathbf{x}, \mathbf{y}) = 2 \arccos(\langle \sqrt{\mathbf{x}}, \sqrt{\mathbf{y}} \rangle),$$

where the square root is meant componentwise. Its tangential space is given by $T_{\mathbf{x}}\mathcal{M} = \{\mathbf{y} \in \mathbb{R}^{d+1} : \langle \mathbf{y}, \mathbf{1} \rangle = 0\}$. The exponential map reads

$$\exp_{\mathbf{x}}(v) = \frac{1}{2} \left(\mathbf{x} + \frac{v_x^2}{\|v_x\|_2^2} \right) + \frac{1}{2} \left(\mathbf{x} - \frac{v_x^2}{\|v_x\|_2^2} \right) \cos(\|v_x\|_2) + \frac{v}{\|v_x\|_2} \sin(\|v_x\|_2),$$

where $v_x := \frac{v}{\sqrt{\mathbf{x}}}$ and vector multiplications are meant componentwise. While the above function maps onto the closure of Δ_d we have to consider only the dense set in $T_{\mathbf{x}}\Delta_d$ with $\exp_{\mathbf{x}}(v) \in \Delta_d$. The logarithmic map is determined by

$$\log_{\mathbf{x}}(\mathbf{y}) = \text{dist}_{\Delta_d}(\mathbf{x}, \mathbf{y}) \frac{\sqrt{\mathbf{x}\mathbf{y}} - \langle \sqrt{\mathbf{x}}, \sqrt{\mathbf{y}} \rangle \mathbf{x}}{\sqrt{1 - \langle \sqrt{\mathbf{x}}, \sqrt{\mathbf{y}} \rangle^2}}.$$

An orthonormal basis can be constructed by taking a basis of $T_{\mathbf{x}}\mathcal{M}$, e.g.,

$$\{(1, -1, 0, 0, \dots)^T, (1, 1, -2, 0, \dots)^T, \dots, (1, 1, \dots, 1, -d)^T\} \subset \mathbb{R}^{d+1}.$$

and applying Gram-Schmidt orthonormalization process w.r.t. the inner product $\langle \cdot, \cdot \rangle_{\mathbf{x}}$.

C. Simulation of Gaussian Noise Model by Said et al. [61]

In the following we explain how to generate samples from the normal distribution $\mathcal{N}_{\text{Said}}(\boldsymbol{\mu}, \sigma^2 I_n)$ on $\text{SPD}(r)$ ($n = \dim(\text{SPD}(r)) = \frac{r(r+1)}{2}$), which was only sketched in [61]. To do so, we parametrize $\mathbf{x} \in \text{SPD}(r)$ by its eigenvalues and eigenvectors (spectral decomposition), given as

$$\mathbf{x}(\rho, \mathbf{u}) = \mathbf{u} \text{diag}(e^{\rho}) \mathbf{u}^T,$$

where $\mathbf{u} \in \text{O}(r)$ is an orthogonal matrix and $\text{diag}(e^{\rho})$ is the diagonal matrix with diagonal $(e^{\rho_1}, \dots, e^{\rho_r})$.

As it is shown in [61], in order to sample from $\mathcal{N}_{\text{Said}}(\boldsymbol{\mu}, \sigma^2 I_n)$ it suffices to generate samples

from $\mathcal{N}_{\text{Said}}(I_r, \sigma^2 I_n)$. Indeed, if $\mathbf{x} \sim \mathcal{N}_{\text{Said}}(I_r, \sigma^2 I_n)$, then $\boldsymbol{\mu}^{\frac{1}{2}} \mathbf{x} (\boldsymbol{\mu}^{\frac{1}{2}})^{\text{T}} \sim \mathcal{N}_{\text{Said}}(\boldsymbol{\mu}, \sigma^2 I_n)$. Further, for sampling from $\mathcal{N}_{\text{Said}}(I_r, \sigma^2 I_n)$ it is enough to sample from the uniform distribution on $O(r)$ to generate \mathbf{u} and from the distribution with density

$$p(\boldsymbol{\rho}) \propto \exp\left\{-\frac{\rho_1^2 + \dots + \rho_r^2}{2\sigma^2}\right\} \prod_{i < j} \sinh\left(\frac{|\rho_i - \rho_j|}{2}\right) \quad (27)$$

to generate $\boldsymbol{\rho}$. Once these are obtained, they can be plugged into the spectral decomposition $\mathbf{x} = \mathbf{x}(\boldsymbol{\rho}, \mathbf{u})$ to obtain $\mathbf{x} \sim \mathcal{N}(I_r, \sigma^2 I_n)$.

Sampling from the uniform distribution on $O(r)$ can be done using a matrix A whose components are i.i.d. standard normally distributed. Computing the QR-decomposition $\mathbf{a} = \mathbf{u}\mathbf{r}$ with \mathbf{u} orthogonal and \mathbf{r} upper triangular, \mathbf{u} is uniformly distributed on $O(r)$, see, e.g., [20].

Sampling from the multivariate density f in (27) can be achieved using the *acceptance-rejection* method, see, e.g., [58]. As dominating density we choose the density of the Euclidean Gaussian distribution $\mathcal{N}(0, \tilde{\sigma}^2 I_r)$, where $\tilde{\sigma}^2 = \frac{2\sigma^2}{2-2(r-1)\sigma^2}$. As we need $\tilde{\sigma}^2 > 0$, this allows only to sample in the case where $\sigma^2 < \frac{1}{r-1}$. However, numerical experiments indicate that this completely suffices to generate realistic Gaussian noise matrices which might arise in applications. In order to use the acceptance-rejection method we have to show that $\frac{f(\boldsymbol{\rho})}{g(\boldsymbol{\rho})} \leq C$ for some constant $C > 0$, where f is proportional to the density we want to sample from and g is proportional to the chosen dominating density. In our situation, we choose

$$g(\boldsymbol{\rho}) = \exp\left\{-\frac{\rho_1^2 + \dots + \rho_r^2}{2\tilde{\sigma}^2}\right\} \propto \frac{1}{(2\pi\tilde{\sigma}^2)^{\frac{r}{2}}} \exp\left\{-\frac{\rho_1^2 + \dots + \rho_r^2}{2\tilde{\sigma}^2}\right\}.$$

To show $\frac{f(\boldsymbol{\rho})}{g(\boldsymbol{\rho})} \leq C$, we first estimate

$$\begin{aligned} \prod_{i < j} \sinh\left(\frac{|\rho_i - \rho_j|}{2}\right) &= \prod_{i \neq j} \left[\sinh\left(\frac{|\rho_i - \rho_j|}{2}\right) \right]^{\frac{1}{2}} = \prod_{i \neq j} \left[\frac{1}{2} \left(e^{\frac{|\rho_i - \rho_j|}{2}} - e^{-\frac{|\rho_i - \rho_j|}{2}} \right) \right]^{\frac{1}{2}} \\ &\leq 2^{-\frac{r(r-1)}{2}} \prod_{i \neq j} e^{\frac{|\rho_i - \rho_j|}{4}} = 2^{-\frac{r(r-1)}{2}} \exp\left\{\frac{1}{4} \sum_{i \neq j} |\rho_i - \rho_j|\right\} \\ &\leq 2^{-\frac{r(r-1)}{2}} \exp\left\{\frac{1}{4} \sum_{i \neq j} |\rho_i| + |\rho_j|\right\} = 2^{-\frac{r(r-1)}{2}} \exp\left\{\frac{r-1}{2} \sum_{i=1}^r |\rho_i|\right\}. \end{aligned}$$

Using

$$\begin{aligned} \exp\left\{-\frac{1}{2\tilde{\sigma}^2} \sum_{i=1}^r \rho_i^2\right\} &= \exp\left\{-\frac{2-2(r-1)\sigma^2}{4\sigma^2} \sum_{i=1}^r \rho_i^2\right\} \\ &= \exp\left\{-\frac{1}{2\sigma^2} \sum_{i=1}^r \rho_i^2\right\} \exp\left\{\frac{2(r-1)}{4} \sum_{i=1}^r \rho_i^2\right\} \end{aligned}$$

we finally obtain

$$\begin{aligned} \frac{f(\rho)}{g(\rho)} &\leq \frac{2^{-\frac{r(r-1)}{2}} \exp\left\{-\frac{1}{2\sigma^2} \sum_{i=1}^r \rho_i^2\right\} \exp\left\{\frac{r-1}{2} \sum_{i=1}^r |\rho_i|\right\}}{\exp\left\{-\frac{1}{2\sigma^2} \sum_{i=1}^r \rho_i^2\right\} \exp\left\{\frac{r-1}{2} \sum_{i=1}^r \rho_i^2\right\}} \\ &= 2^{-\frac{r(r-1)}{2}} \exp\left\{\frac{r-1}{2} \sum_{i=1}^r \underbrace{|\rho_i| - \rho_i^2}_{\leq \frac{1}{4}}\right\} \\ &\leq C, \end{aligned}$$

where $C = e^{\frac{r(r-1)}{8}} 2^{-\frac{r(r-1)}{2}} > 0$.

Acknowledgments We would like to thank R. Bergmann for fruitful discussions and for providing the test image in Figure 7. Funding by the German Research Foundation (DFG) within the project STE 571/13-1 is gratefully acknowledged.

References

- [1] B. AFSARI, *Riemannian L^p center of mass: Existence, uniqueness, and convexity*, Proceedings of the American Mathematical Society, 139 (2011), pp. 655–673.
- [2] B. AFSARI, R. TRON, AND R. VIDAL, *On the convergence of gradient descent for finding the Riemannian center of mass*, SIAM Journal on Control and Optimization, 51 (2013), pp. 2230–2260.
- [3] C. AGUERREBERE, A. ALMANSA, J. DELON, Y. GOUSSEAU, AND P. MUSÉ, *Inverse Problems in Imaging: a Hyperprior Bayesian Approach*, Preprint HAL 01107519, (2016).
- [4] F. J. ANSCOMBE, *The transformation of Poisson, binomial and negative-binomial data*, Biometrika, 35 (1948), pp. 246–254.
- [5] V. ARSIGNY, P. FILLARD, X. PENNEC, AND N. AYACHE, *Fast and simple calculus on tensors in the Log-Euclidean framework*, in International Conference on Medical Image Computing and Computer-Assisted Intervention, vol. 3749, Springer, 2005, pp. 115–122.
- [6] M. BAČÁK, *Convex Analysis and Optimization in Hadamard Spaces*, vol. 22 of De Gruyter Series in Nonlinear Analysis and Applications, De Gruyter, Berlin, 2014.
- [7] M. BAČÁK, R. BERGMANN, G. STEIDL, AND A. WEINMANN, *A second order non-smooth variational model for restoring manifold-valued images*, SIAM Journal on Scientific Computing, 38 (2016), pp. 567–597.
- [8] F. BACHMANN, R. HIELSCHER, AND H. SCHAEUBEN, *Grain detection from 2d and 3d EBSD data - Specification of the MTEX algorithm*, Ultramicroscopy, 111 (2011), pp. 1720–1733.

- [9] R. BERGMANN, R. H. CHAN, R. HIELSCHER, J. PERSCH, AND G. STEIDL, *Restoration of manifold-valued images by half-quadratic minimization*, Inverse Problems in Imaging, 10 (2016), pp. 281–304.
- [10] R. BERGMANN, F. LAUS, G. STEIDL, AND A. WEINMANN, *Second order differences of cyclic data and applications in variational denoising*, SIAM Journal on Imaging Sciences, 7 (2014), pp. 2916–2953.
- [11] R. BERGMANN AND A. WEINMANN, *A second order TV-type approach for inpainting and denoising higher dimensional combined cyclic and vector space data*, Journal of Mathematical Imaging and Vision, 55 (2016), pp. 401–427.
- [12] R. BHATTACHARYA AND V. PATRANGENARU, *Large sample theory of intrinsic and extrinsic sample means on manifolds I*, Annals of Statistics, (2003), pp. 1–29.
- [13] J. BIOUCAS-DIAS, V. KATKOVNIK, J. ASTOLA, AND K. EGIAZARIAN, *Absolute phase estimation: adaptive local denoising and global unwrapping*, Applied Optics, 47 (2008), pp. 5358–5369.
- [14] A. BUADES, B. COLL, AND J.-M. MOREL, *On image denoising methods*, SIAM Multiscale Modeling and Simulation, 4 (2005), pp. 490–530.
- [15] T. F. CHAN, S. KANG, AND J. SHEN, *Total variation denoising and enhancement of color images based on the CB and HSV color models*, Journal of Visual Communication and Image Representation, 12 (2001), pp. 422–435.
- [16] P. CHATTERJEE AND P. MILANFAR, *Is denoising dead?*, IEEE Transactions on Image Processing, 19 (2010), pp. 895–911.
- [17] ———, *Patch-based near-optimal image denoising*, IEEE Transactions on Image Processing, 21 (2012), pp. 1635–1649.
- [18] C. CHEFD’HOTEL, D. TSCHUMPERLÉ, R. DERICHE, AND O. FAUGERAS, *Regularizing flows for constrained matrix-valued images*, Journal of Mathematical Imaging and Vision, 20 (2004), pp. 147–162.
- [19] E. CHEVALLIER, K. KALUNGA, AND J. ANGULO, *Kernel density estimation on spaces of gaussian distribution and symmetric positive definite matrices*, HAL Preprint, hal-01245712, (2015).
- [20] Y. CHIKUSE, *Statistics on Special Manifolds*, vol. 174, Springer Science & Business Media, 2012.
- [21] K. DABOV, A. FOI, V. KATKOVNIK, AND K. EGIAZARIAN, *Image restoration by sparse 3d transform-domain collaborative filtering*, in Electronic Imaging 2008, International Society for Optics and Photonics, 2008, pp. 681207–681207.
- [22] ———, *BM3D image denoising with shape-adaptive principal component analysis*, in SPARS’09-Signal Processing with Adaptive Sparse Structured Representations, Saint-Malo, France, 2009.

- [23] C.-A. DELEDALLE, L. D., AND F. TUPIN, *Iterative weighted maximum likelihood denoising with probabilistic patch-based weights*, IEEE Transactions on Image Processing, 18 (2009), pp. 2661–2672.
- [24] C.-A. DELEDALLE, L. DENIS, AND F. TUPIN, *NL-InSAR: Nonlocal interferogram estimation*, IEEE Transactions on Geoscience Remote Sensing, 49 (2011), pp. 1441–1452.
- [25] M. DUERINCKX, C. LEY, AND Y. SWAN, *Maximum likelihood characterization of distributions*, Bernoulli, 20 (2014), pp. 775–802.
- [26] M. ELAD AND M. AHARON, *Image denoising via sparse and redundant representations over learned dictionaries*, IEEE Transactions on Image Processing, 15 (2006), pp. 3736–3745.
- [27] J. A. FESSLER, *Image Reconstruction: Algorithms and Analysis*.
- [28] P. T. FLETCHER AND S. J., *Principal geodesic analysis on symmetric spaces: Statistics of diffusion tensors*, in Computer Vision and Mathematical Methods in Medical and Biomedical Image Analysis, vol. 3117, Springer, 2004, pp. 87–98.
- [29] W. FREEDEN, T. GERVENES, AND M. SCHREINER, *Constructive Approximation on the Sphere*, Clarendon Press, Oxford, 1998.
- [30] G. GILBOA AND S. OSHER, *Nonlocal operators with applications to image processing*, SIAM Journal on Multiscale Modeling and Simulation, 7 (2008), pp. 1005–1028.
- [31] R. C. GONZALEZ AND P. WOODS, *Digital Image Processing*, Addison–Wesley, Reading, third ed., 2008.
- [32] M. GRÄF, D. POTTS, AND G. STEIDL, *Quadrature rules, discrepancies, and their relations to halftoning on the torus and the sphere*, SIAM Journal on Scientific Computing, 34 (2012), pp. A2760–A2791.
- [33] A. GRIGOR’YAN, *Kernel and Analysis on Manifolds*, American Mathematical Society, 2009.
- [34] E. J. GUMBEL, J. A. GREENWOOD, AND D. DURAND, *The circular normal distribution: theory and tables*, Journal of the American Statistical Society, 48 (1953), pp. 131–152.
- [35] I. H. JERMYN, *Invariant Bayesian estimation on manifolds*, Annals of Statistics, (2005), pp. 583–605.
- [36] H. KARCHER, *Riemannian center of mass and mollifier smoothing*, Communications on Pure and Applied Mathematics, 30 (1977), pp. 509–541.
- [37] W. S. KENDALL, *Probability, convexity and harmonic maps with small images i: uniqueness and fine existence*, Proceedings of The London Mathematical Society, 61 (1990), pp. 371–406.

- [38] C. KERVRANN, *Pewa: Patch-based exponentially weighted aggregation for image denoising*, in Advances in Neural Information Processing Systems, Curran Associates, Inc., 2014, pp. 2150–2158.
- [39] R. KIMMEL AND N. SOCHEN, *Orientation diffusion or how to comb a porcupine*, Journal of Visual Communication and Image Representation, 13 (2002), pp. 238–248.
- [40] M. LEBRUN, A. BUADES, AND J. M. MOREL, *Implementation of the “Non-Local Bayes” (NL-Bayes) Image Denoising Algorithm*, Image Processing On Line, 3 (2013), pp. 1–42.
- [41] M. LEBRUN, A. BUADES, AND J.-M. MOREL, *A nonlocal Bayesian image denoising algorithm*, SIAM Journal on Imaging Sciences, 6 (2013), pp. 1665–1688.
- [42] M. LEBRUN, M. COLOM, A. BUADES, AND J. MOREL, *Secrets of image denoising cuisine*, Acta Numerica, 21 (2012), pp. 475–576.
- [43] E. L. LEHMANN AND G. CASELLA, *Theory of point estimation*, Springer Science & Business Media, 2006.
- [44] E. L. LEHMANN AND H. SCHEFFÉ, *Completeness, similar regions, and unbiased estimation: Part I*, Sankhyā: the Indian Journal of Statistics, (1950), pp. 305–340.
- [45] ———, *Completeness, similar regions, and unbiased estimation: Part II*, Sankhyā: The Indian Journal of Statistics (1933-1960), 15 (1955), pp. 219–236.
- [46] J. LELLMANN, E. STREKALOVSKIY, S. KOETTER, AND D. CREMERS, *Total variation regularization for functions with values in a manifold*, in Proceedings of the IEEE International Conference on Computer Vision, 2013, pp. 2944–2951.
- [47] A. LEVIN AND B. NADLER, *Natural image denoising: Optimality and inherent bounds*, in IEEE Conference on Computer Vision and Pattern Recognition (CVPR), IEEE, 2011, pp. 2833–2840.
- [48] K. V. MARDIA AND P. E. JUPP, *Directional Statistics*, vol. 494, John Wiley & Sons, Wiley, C., 2000.
- [49] G. MATEU-FIGUERAS, V. PAWLOWSKY-GLAHN, AND J. J. EGOZCUE, *The normal distribution in some constrained sample spaces*, Statistics and Operation Research Transactions, 37 (2013), pp. 29–56.
- [50] Y.-I. OHTA, T. KANADE, AND T. SAKAI, *Color information for region segmentation*, Computer Graphics Image Processing, 13 (1980), pp. 222–241.
- [51] J. M. OLLER AND J. M. CORCUERA, *Intrinsic analysis of statistical estimation*, The Annals of Statistics, 23 (1995), pp. 1562–1582.
- [52] V. PAPYAN AND M. ELAD, *Multi-scale patch-based image restoration*, IEEE Transactions on Image Processing, 25 (2016), pp. 249–261.
- [53] X. PENNEC, *Intrinsic statistics on Riemannian manifolds: Basic tools for geometric measurements*, Journal of Mathematical Imaging and Vision, 25 (2006), pp. 127–154.

- [54] X. PENNEC, P. FILLARD, AND N. AYACHE, *A Riemannian framework for tensor computing*, International Journal of Computer Vision, 66 (2006), pp. 41–66.
- [55] L. PIZARRO, B. BURGETH, S. DIDAS, AND J. WEICKERT, *A generic neighbourhood filtering framework for matrix fields*, in European Conference on Computer Vision, Springer, 2008, pp. 521–532.
- [56] I. RAM, M. ELAD, AND I. COHEN, *Patch-ordering-based wavelet frame and its use in inverse problems*, IEEE Transactions on Image Processing, 23 (2014), pp. 2779–2792.
- [57] R. REBONATO AND P. JÄCKEL, *The most general methodology to create a valid correlation matrix for risk management and option pricing purposes*, Available at SSRN 1969689, (2011).
- [58] C. ROBERT AND G. CASELLA, *Monte Carlo Statistical Methods*, Springer Science & Business Media, 2013.
- [59] G. ROSMAN, M. BRONSTEIN, A. BRONSTEIN, A. WOLF, AND R. KIMMEL, *Group-valued regularization framework for motion segmentation of dynamic non-rigid shapes*, in Scale Space and Variational Methods in Computer Vision, Springer, 2012, pp. 725–736.
- [60] L. I. RUDIN, S. OSHER, AND E. FATEMI, *Nonlinear total variation based noise removal algorithms*, Physica D, 60 (1992), pp. 259–268.
- [61] S. SAID, L. BOMBRUN, Y. BERTHOUMIEU, AND J. H. MANTON, *Riemannian Gaussian distributions on the space of symmetric positive definite matrices*, arXiv preprint arXiv:1507.01760, accepted in IEEE Transactions on Information Theory, (2015).
- [62] S. SAID, H. HAJRI, L. BOMBRUN, AND B. C. VEMURI, *Gaussian distributions on Riemannian symmetric spaces: statistical learning with structured covariance matrices*, arXiv preprint arXiv:1607.06929, (2016).
- [63] J. SALMON, *On two parameters for denoising with non-local means*, IEEE Signal Processing Letters, 17 (2010), pp. 269–272.
- [64] J. SAMON, C. A. DELEDALLE, AND A. DALALYAN, *Image denoising with patched based PCA*, in Proceedings of the British Machine Vision Conference, Cambridge, UK, 2011, BMVA Press, pp. 25.1–25.10–10.
- [65] W. STADJE, *ML characterization of the multivariate normal distribution*, Journal of Multivariate Analysis, 46 (1993), pp. 131–138.
- [66] E. STREKALOVSKIY AND D. CREMERS, *Total cyclic variation and generalizations*, Journal of Mathematical Imaging and Vision, 47 (2013), pp. 258–277.
- [67] A. TERRAS, *Harmonic Analysis on Symmetric Spaces and Applications II*, Springer-Verlag, New York, 1988.
- [68] O. TUZEL, F. PORIKLI, AND P. MEER, *Learning on Lie groups for invariant detection and tracking*, in CVPR 2008, IEEE, 2008, pp. 1–8.

- [69] T. VALKONEN, K. BREDIES, AND F. KNOLL, *Total generalized variation in diffusion tensor imaging*, SIAM Journal on Imaging Sciences, 6 (2013), pp. 487–525.
- [70] L. A. VESE AND S. J. OSHER, *Numerical methods for p -harmonic flows and applications to image processing*, SIAM Journal on Numerical Analysis, 40 (2002), pp. 2085–2104.
- [71] R. VON MISES, *Magnetisme et theorie des atoms*, Annalles de Chimie et de Physique, 5 (1905), pp. 71–127.
- [72] ———, *Über die Ganzzahligkeit der Atomgewichte und verwandte Fragen*, Physikalische Zeitschrift, 19 (1918), pp. 490–500.
- [73] Y. WANG, *E-PLE: an Algorithm for Image Inpainting*, Image Processing On Line, 3 (2013), pp. 271–285.
- [74] Y.-Q. WANG AND J.-M. MOREL, *Sure guided gaussian mixture image denoising*, SIAM Journal on Imaging Sciences, 6 (2013), pp. 999–1034.
- [75] J. WEICKERT, C. FEDDERN, M. WELK, B. BURGETH, AND T. BROX, *PDEs for tensor image processing*, in Visualization and Processing of Tensor Fields, Berlin, 2006, Springer, pp. 399–414.
- [76] A. WEINMANN, L. DEMARET, AND M. STORATH, *Total variation regularization for manifold-valued data*, SIAM Journal on Imaging Sciences, 7 (2014), pp. 2226–2257.
- [77] N. WIEST-DAESSLÉ, S. PRIMA, P. COUPÉ, S. P. MORRISSEY, AND C. BARILLOT, *Non-local means variants for denoising of diffusion-weighted and diffusion tensor MRI*, in International Conference on Medical Image Computing and Computer-Assisted Intervention, vol. 4792, Springer, 2007, pp. 344–351.
- [78] L. P. YAROSLACSKY, K. O. EGIAZARIAN, AND J. T. ASTOLA, *Transform domain image restoration methods: review, comparison and interpretation*, in Proceedings of SPIE 4303, 2001, p. 155.
- [79] L. P. YAROSLAVSKY, *Theoretical Foundations of Digital Imaging Using MATLAB®*, CRC Press, 2012.
- [80] G. YU, G. SAPIRO, AND S. MALLAT, *Solving inverse problems with piecewise linear estimators: From Gaussian mixture models to structured sparsity*, IEEE Transactions on Image Processing, 21 (2012), pp. 2481–2499.
- [81] D. ZORAN AND Y. WEISS, *From learning models of natural image patches to whole image restoration*, in IEEE International Conference on Computer Vision (ICCV), Washington, DC, 2011, IEEE, pp. 479–486.